Computational studies on new chemical species in the gas-phase and the solid-state.

Dissertation for the degree of Doctor Philosophiae

Patryk Zaleski-Ejgierd

University of Helsinki
Department of Chemistry
Laboratory for Instruction in Swedish
P.O. Box 55 (A.I. Virtasen Aukio 1)
FIN-00014 University of Helsinki, Finland

To be presented, with permission of the Faculty of Science, University of Helsinki, for public discussion in Auditorium CK112, Exactum (Gustaf Hällströmin katu 2, Helsinki), September 9th, 2009, at 2:00 pm.

Helsinki 2009

Supervised by

Prof. Pekka Pyykkö
Department of Chemistry
University of Helsinki
Helsinki, Finland

Reviewed by

Prof. Hannu Häkkinen
Departments of Physics and Chemistry
Nanoscience Center
University of Jyväskylä
Jyväskylä, Finland

Prof. Peter Schwerdtfeger
Centre for Theoretical Chemistry and Physics
New Zealand Institute for Advanced Study
Massey University
Auckland, New Zeland

ISBN 978-952-92-5917-5 (paperback)
ISBN 978-952-10-5674-1 (PDF)
http://ethesis.helsinki.fi

Yliopistopaino Helsinki 2009

"The more you know, the harder it is to take decisive action. Once you become informed, you start seeing complexities and shades of gray. You realize that nothing is as clear and simple as it first appears."

— Bill Watterson, Calvin & Hobbe

The research for this thesis has been carried out at the Laboratory for Instruction in Swedish, Department of Chemistry, University of Helsinki during the time from August 2006 to September 2009.

All the presented work was conducted under the supervision of Professor Pekka Pyykkö. I wish to express my thankfulness to Pekka for giving me the opportunity to work with him, for his time and professional scientific support. After the three years I can't recall him ever saying *"No"* to me — *Pekka, I owe my gratitude to you and for that I sincerely thank you.*

I want to thank my co-authors: Mikko Hakala and Michael Patzschke. Working with you was a pleasure. I also thank the reviewers of my thesis: Professor Hannu Häkkinen and Professor Peter Schwerdtfeger. You valuable comments certainly increased value of my thesis.

Much of this work would have been more difficult without the encouragement and support from the rest of the people working at the Department of Chemistry. — *Dear Michiko Atsumi, Raija Eskelinen, Ying-Chan Lin, Susanne Lundberg, Anette Rojano Rosales, Anneka Tuomola, Nina Siegfrids, Gustav Boije af Gennäs, Krister Henriksson, Jonas Jusélius, Olli Lehtonen, Sergio Losilla, Mikael Johansson, Jesús Muñiz, Michael Patzschke, Janne Pesonen, Sebastian Riedel, Nino Runeberg, Michal Straka, Dage Sundholm, Stefan Taubert, Juha Vaara, Tommy Vänskä, Bertel Westermark and Cong Wang — I hereby thank you all for the discussions ... and arguments, for your support, help and the strength you gave, when I needed it most.*

Michiko and Ying-Chan, *I cordially thank you* for your support and conversations we had. They were very helpful and important to me and my future decisions.

Dage, I was always looking forward to your advices and constructive remarks concerning my research — *Thank you.*

Mikael and Michael, you were both here when I started, you are both here when I finish, and you are both nice friends whom I enjoyed talking to — *Thanks.*

Sergio, *many thanks* for your Spanish attitude and your sense of humor. You always knew how to cheer me up.

Cong, I regret we never had opportunity to work on the same project. I'm sure it would have been very fruitful and interesting. — *Cong, thank you for being a good friend!*

Finally, I want to express my *deepest gratitude* to Anna Olszewska. Dear Ania, you should be a co-author of this thesis. We both know I would have not finished it without you standing by me.

In addition to personal contributions, the Finnish Centre for Scientific Computing (CSC) is acknowledged for providing computational resources. The following institutions are acknowledged for providing financial support:

- University of Helsinki
- Finnish Centre of Excellence in Computational Molecular Science
- Magnus Ehrnrooth Foundation
- Finnish Cultural Foundation
- Svenska Tekniska Vetenskapsakademien i Finland
- Alfred Kordelin Foundation (Gust. Komppa fund)
- Laskennallisen Kemian ja Molekyylispektroskopian Tutkijakoulu (LasKeMo)

— Patryk Zaleski-Ejgierd, Helsinki 07.08.09

Dla Ani

Abstract

There is intense activity in the area of theoretical chemistry of gold.[1,2] It is now possible to predict new molecular species, and more recently, solids by combining relativistic methodology with isoelectronic thinking.

In this thesis we predict a series of solid sheet-type crystals for Group-11 cyanides, MCN (M=Cu, Ag, Au), and Group-2 and 12 carbides MC_2 (M=Be-Ba, Zn-Hg). The idea of sheets is then extended to nanostrips which can be bent to nanorings. The bending energies and deformation frequencies can be systematized by treating these molecules as an elastic bodies. In these species Au atoms act as an 'intermolecular glue'. Further suggested molecular species are the new uncongested aurocarbons, and the neutral Au_nHg_m clusters.

Many of the suggested species are expected to be stabilized by aurophilic interactions. We also estimate the MP2 basis-set limit of the aurophilicity for the model compounds $[ClAuPH_3]_2$ and $[P(AuPH_3)_4]^+$. Besides investigating the size of the basis-set applied, our research confirms that the 19-VE TZVP+2f level, used a decade ago, already produced 74 % of the present aurophilic attraction energy for the $[ClAuPH_3]_2$ dimer. Likewise we verify the preferred C_{4v} structure for the $[P(AuPH_3)_4]^+$ cation at the MP2 level. We also perform the first calculation on model aurophilic systems using the SCS-MP2 method and compare the results to high-accuracy CCSD(T) ones.

The recently obtained high-resolution microwave spectra on MCN molecules (M=Cu, Ag, Au) provide an excellent testing ground for quantum chemistry. MP2 or CCSD(T) calculations, correlating all 19 valence electrons of Au and including BSSE and SO corrections, are able to give bond lengths to 0.6 pm, or better. Our calculated vibrational frequencies are expected to be better than the currently available experimental estimates. Qualitative evidence for multiple Au-C bonding in triatomic AuCN is also found.

List of Publications

List of publications included in the thesis

I. Zaleski-Ejgierd, P.; Hakala, M. O.; Pyykkö P. "Comparison of chain versus sheet crystal structures for the cyanides MCN (M=Cu-Au) and dicarbides MC_2 (M=Be-Ba, Zn-Hg)", *Phys. Rev. B* **2007**, *76*, 094104.

II. Pyykkö P.; M. O. Hakala; and Zaleski-Ejgierd, P. "Gold as intermolecular glue: a theoretical study of nanostrips based on quinoline-type monomers", *Phys. Chem. Chem. Phys.* **2007**, *9*, 3025.

III. Pyykkö P.; Zaleski-Ejgierd, P. "From nanostrips to nanorings: A comparison of gold-glued polyauronaphthyridines with polyacenes", *Phys. Chem. Chem. Phys.* **2008**, *10*, 114.

IV. Pyykkö P.; Zaleski-Ejgierd, P. "Basis-set limit of the aurophilic attraction using the MP2 method. The examples of $[ClAuPH_3]_2$ dimer and $[P(AuPH_3)_4]^+$ ion", *J. Chem. Phys.* **2008**, *128*, 124309.

V. Zaleski-Ejgierd, P.; Patzschke M.; Pyykkö P. "Structure and bonding of the MCN molecules, M=Cu, Ag, Au, Rg", *J. Chem. Phys.* **2008**, *128*, 224303.

VI. Zaleski-Ejgierd, P.; Pyykkö P. "Au_nHg_m clusters: mercury aurides, gold amalgams, or van der Waals aggregates?", *J. Phys. Chem. A* **2009**, Article ASAP, DOI: 10.1021/jp810423j.

VII. Zaleski-Ejgierd, P.; Pyykkö P. "Bonding analysis for sterically uncongested, simple aurocarbons C_nAu_m", *Can. J. Chem.* **2009**, *87*, 798.

Contents

List of Abbreviations

AO	Atomic Orbital
BO	Born-Oppenheimer
BODC	Born-Oppenheimer Diagonal Correction
CC	Coupled-Cluster
CI	Configuration Interaction
CP	Counterpoise Correction
DCB	Dirac-Coulomb-Breit
DFT	Density Functional Theory
DK	Douglas-Kroll
DOS	Density of States
DZ	Double Zeta
FBZ	First Brillouin Zone
LCAO	Linear Combination of Atomic Orbitals
LHS	Left-Hand Side
LDA	Local Density Approximation
LSDA	Local Spin Density Approximation
GGA	Generalized Gradient Approximation
HF	Hartree-Fock
IOTC	Infinite-Order Two-Component
F-W	Foldy-Wouthuysen
FBZ	First Brillouin Zone
FORA	First-Order Regular Approximation
GTO	Gaussian Type Orbitals
MP2	Second-order Møller-Plesset
PES	Potential Energy Surface
PP	Pseudo-Potential
PW	Plane-Wave
QZ	Quadruple Zeta
RI	Resolution of the Identity
SCF	Self-Consistent Field
STO	Slater Type Orbital
SV	Split-Valence
TZ	Triple Valence Zeta
WFT	Wave-Function Theory
ZORA	Zeroth-Order Regular Approximation
X2C	Exact Two-Component

bcc	body-centered cubic
fcc	face-centered cubic
hex	hexagonal
cc	correlation-consistent
pGTO	primitive GTO
pSTO	primitive STO
sc	simple cubic
vdW	van der Waals

Chapter 1

Introduction

1.1 Historical background

During the 19th century, various phenomena were observed that could not be explained by classical physics, see Table 1.1. Planck showed in 1900 that the intensity of black-body radiation,

$$I(\nu, T)d\nu = \frac{2h\nu^3}{c^2}\frac{1}{e^{\frac{h\nu}{kT}} - 1}\, d\nu \tag{1.1}$$

decays for high energies, if $h\nu/kT \gg 1$. The electromagnetic radiation takes place as quanta, whose energy is $\Delta E = h\nu$. On the other hand, these energy differences arise from discrete energy levels,

$$\Delta E = E_i - E_f. \tag{1.2}$$

This is implicit in the spectral formulae of Balmer, Rydberg, $etc.$, and was explicitly introduced by Bohr.

The energies of the bound states are quantized. They are determined as the eigenvalues, E_i, of the differential equation

$$H\Psi_i = E_i\Psi_i. \tag{1.3}$$

Here H is the Hamiltonian (the operator corresponding to the total energy) and Ψ_i is the wave function of state i of the physical system. For a single particle moving in a potential V we have,

$$H = T + V, \tag{1.4}$$

and

$$T = -\frac{\hbar^2}{2m}\nabla^2. \tag{1.5}$$

The origin (1.3) of the quantization was found independently by Heisenberg, Schrödinger and Dirac. For time-dependent problems the eigenvalue problem is defined as:

$$H\Psi_i = i\hbar\frac{\partial}{\partial\, t}\Psi_i. \tag{1.6}$$

Phenomenon	Discovery	Models
Spectral lines	(1814) Fraunhofer	Balmer, Rydberg, Bohr, Schrödinger
Covalent-bonding	∼(1828) Berzelius	Heitler-London
Black-body radiation	(1862) Kirchoff	Wien, Rayleigh-Jeans, Planck
Photoelectric effect	(1902) von Lenard	Einstein
Compton effect	(1923) Compton	

Table 1.1: Phenomena requiring quantum mechanics.

For relativistic particles with spin $\frac{1}{2}$ one keeps the equations (1.3) and (1.6) but replaces the non-relativistic H (1.4) by the relativistic Dirac Hamiltonian H_D, see Chapter 6.

Many-electron problems can be approached using Wave-Function Theory (WFT, Chapter 2) or Density-Functional Theory (DFT, Chapter 3).

Chapter 2

Wave-Function Theory

2.1 The N-electron Schrödinger equation

Consider an N-electron system. The electronic Hamiltonian, expressed in atomic units, is taken as

$$H = \sum_{i}^{N} h_i + \sum_{i>j}^{N} h_{ij} \tag{2.1}$$

where the operators h_i and h_{ij} are defined as

$$h_i = -\frac{1}{2}\nabla_i^2 - \sum_{a}^{A} \frac{Z_a}{r_{ia}}, \qquad h_{ij} = \frac{1}{r_{ij}} = V_{ij}. \tag{2.2}$$

A wave-function, Ψ, satisfying the antisymmetry requirements

$$\Psi(i,j) = -\Psi(j,i) \tag{2.3}$$

for the exchange of electrons i and j, can be approximated by a Slater determinant

$$\Psi = \frac{1}{N!^{\frac{1}{2}}} \begin{vmatrix} \varphi_1(1) & \varphi_2(1) & \dots & \varphi_N(1) \\ \varphi_1(2) & \varphi_2(2) & \dots & \varphi_N(2) \\ \dots & \dots & \dots & \dots \\ \varphi_1(N) & \varphi_2(N) & \dots & \varphi_N(N) \end{vmatrix}. \tag{2.4}$$

The electronic energy, E_{el}, can be calculated as the expectation value

$$E_{el} = \langle \Psi | H | \Psi \rangle . \tag{2.5}$$

For a closed-shell system this yields

$$E_{el} = 2\sum_{i=1}^{N/2} h_{ii} + \sum_{i=1}^{N/2}\sum_{j=1}^{N/2}(2J_{ij} - K_{ij}), \tag{2.6}$$

where h_{ii} is the sum of average kinetic and potential energy of the electrostatic attraction between the nuclei and the electron i,

$$h_{ii} = \langle \varphi_i(1)| - \frac{1}{2}\nabla^2(1) - \sum_a^A \frac{Z_a}{r_{1a}} |\varphi_i(1)\rangle \,, \tag{2.7}$$

the Coulomb integral

$$J_{ij} = \langle \varphi_i(1)\varphi_j(2)| \frac{1}{r_{12}} |\varphi_i(1)\varphi_j(2)\rangle \,, \tag{2.8}$$

describes the potential energy for the electrostatic repulsion between two electrons, and the exchange integral

$$K_{ij} = \langle \varphi_i(1)\varphi_j(2)| \frac{1}{r_{12}} |\varphi_i(2)\varphi_j(1)\rangle \tag{2.9}$$

arises from the requirement that Ψ be antisymmetric with respect to the permutation of any two coordinates.

2.1.1 The Hartree-Fock method

In the first approximation, the exact wave-function of a given state can be approximated by a single Slater determinant. Since the energy expression (2.6) is stationary with respect to small variations in the orbitals φ, the variational approach may be applied to find the set of orbitals that minimizes the value of E_{el}. According to the variational theorem, the wave-function constructed from such orbitals is guaranteed to yield the lowest possible energy within the single-determinant picture and within a given set of orbitals.

The goal of the Hartree-Fock procedure is to minimize the total electronic energy by introducing infinitesimal changes to the initial orbitals

$$\varphi_i \rightarrow \varphi_i + \delta\varphi_i.$$

The minimization procedure typically employs Lagrange's method of undetermined multipliers. The $L[\{\varphi_i\}]$ functional is introduced. By following the variational requirement $\delta L = 0$, a set of N equations defining the optimal orbitals is obtained. The Hartree-Fock equations are given as

$$F(1)\varphi_i(1) = \epsilon_i \varphi_i(1), \tag{2.10}$$

where the ϵ_i values act as the undetermined multipliers, and $F(1)$ is the Fock operator

$$F(1) = \left[-\frac{1}{2}\nabla(1)^2 - \sum_a^A \frac{Z_a}{r_{1a}} \right] + \sum_{j=1}^{N/2} \left(2J_j(1) - K_j(1) \right). \tag{2.11}$$

Here the Coulomb operator $J_j(1)$ is given as

$$J_j(1) = \langle \varphi_j(2)| \frac{1}{r_{12}} |\varphi_j(2)\rangle \,, \tag{2.12}$$

while the exchange operator $K_j(1)$ is defined with respect to the orbital upon which it operates

$$K_j(1)\varphi_i(1) = \left[\langle\varphi_j(2)|\,\frac{1}{r_{12}}\,|\varphi_i(2)\rangle\right]\varphi_j(1). \tag{2.13}$$

Let us now assume that each molecular orbital φ_i can be approximated by a linear combination of M atomic orbitals (LCAO)

$$\varphi_i = \sum_{\mu=1}^{M} c_{\mu i}\chi_\mu, \tag{2.14}$$

where the χ_μ stand for one-electron basis functions. The atomic orbitals (AO) are typically located at the nuclei, and the $c_{\mu i}$ are the expansion coefficients. Introducing the LCAO to the Hartree-Fock equations results in a new set of equations, now defined in a finite space, spanned by the basis functions χ_μ

$$F(1)\sum_{\mu=1}^{M} c_{\mu i}\chi_\mu = \epsilon_i \sum_{\mu=1}^{M} c_{\mu i}\chi_\mu. \tag{2.15}$$

Multiplying (2.15) by χ_ν and integrating over all space yields

$$\sum_{\mu=1}^{M} c_{\mu i}\left(F_{\nu\mu} - \epsilon_i S_{\nu\mu}\right) = 0 \tag{2.16}$$

where $F_{\nu\mu}$ and $S_{\nu\mu}$ are the elements of the Fock and overlap matrixes respectively:

$$F_{\nu\mu} = \langle\chi_\nu|\,F(1)\,|\chi_\mu\rangle\,, \qquad S_{\nu\mu} = \langle\chi_\nu|\chi_\mu\rangle\,. \tag{2.17}$$

For each value of ν there are M such equations. To obtain the nontrivial solution, the so-called secular determinant must be equal to zero

$$\det\left(F_{\nu\mu} - \epsilon_i S_{\nu\mu}\right) = 0. \tag{2.18}$$

The solutions ϵ_i, are the orbital energies. Each solution for an occupied orbital includes the kinetic energy of the electron in a molecular orbital φ_i and the energies resulting from the interactions with the nuclei and the remaining N-1 electrons. For this reason, the Hartree-Fock method is referred to as a Mean-Field Theory.

In terms of the eigenvalues, the total calculated electronic energy is

$$E_{el} = \sum_{i=1}^{N/2}\left[2\epsilon_i - \sum_{j=1}^{N/2}(2J_{ij} - K_{ij})\right]. \tag{2.19}$$

By adding the internuclear repulsion energy

$$E_{AB} = \sum_{a=1}\sum_{b=a+1}\frac{Z_a Z_b}{R_{ab}}, \tag{2.20}$$

one finally obtains the expression for the total energy of an N-electron system

$$E_{HF} = E_{el} + E_{AB}. \tag{2.21}$$

Due to the orbital dependence of the Fock operator, a solution may only be obtained iteratively. Typically one diagonalises a semiempirical Hamiltonian for an initial solution, and using the initial values of the basis set expansion coefficients, $c_{\mu i}$, one performs subsequent calculations. The resulting orbitals serve as an input for the next cycle. The calculations are performed until a chosen criteria for convergence are fulfilled. In that respect, the Hartree-Fock method is also known as the self-consistent-field (SCF) method.

2.1.2 Limitations of the Hartree-Fock method

The Hartree-Fock method is a serious simplification of the exact solution. The theory is constructed in such a way, that the wave-function is antisymmetric with respect to the exchange of two electron positions. As such, the single-determinant Hartree-Fock wave-function, Ψ_{HF}, satisfies only the obligatory, formal requirements of a non-relativistic fermionic wave-function. Unfortunately, a single-determinant representation is insufficient for an accurate, quantitative description of most chemical systems. The main drawback of the HF method, is that it does not, by definition, include Coulomb electron correlation effects.* For certain cases, such as the aurophilic attraction studied in this thesis, neglecting correlation effects leads to intermolecular repulsion instead of attraction. Nonetheless, even for such difficult cases, the HF method is a useful benchmark and a common starting approximation for more advanced, post-Hartree-Fock methods.

2.2 Post-Hartree-Fock techniques

The Hartree-Fock method has the intrinsic limitation of referring to a single-determinant wave-function Ansatz 2.4. To improve such a wave-function, a perturbative treatment may be applied or the variational principle may be extended to more than one determinant.

2.2.1 Møller-Plesset Perturbation Theory

The Møller-Plesset perturbation theory[3,4] is derived by splitting the usual electronic Hamiltonian, H, into the sum of an unperturbed Hamiltonian, H_0, and a perturbation operator λV:

$$H = H_0 + \lambda V, \tag{2.22}$$

*only the Fermi correlation due to exchange is included in HF theory

where λ is a small, but otherwise arbitrary perturbation parameter, and H_0 is the N-electron Fock operator:

$$H_0 = F = \sum_{i=1}^{N} F(i) = \sum_{i=1}^{N} \left(h(i) + \sum_{j=1}^{N/2} [2J_j(i) - K_j(i)] \right). \tag{2.23}$$

The perturbation potential, V, is defined as

$$V = H - H_0 = H - F, \tag{2.24}$$

where F is the Fock operator.

In the Møller-Plesset perturbation theory the wave-function and the energy expression are being expanded into a power series with respect to the parameter λ:

$$\Psi = \Psi^{(0)} + \lambda\Psi^{(1)} + \ldots + \lambda^i\Psi^{(i)} = \sum_{i=0}^{n} \lambda^i\Psi^{(i)} \tag{2.25}$$

$$E = E^{(0)} + \lambda E^{(1)} + \ldots + \lambda^i E^{(i)} = \sum_{i=0}^{n} \lambda^i E^{(i)} \tag{2.26}$$

A simple substitution of equations (2.22), (2.25) and (2.26) into the Schrödinger equation results in the perturbation equation

$$(H_0 + \lambda V) \left(\sum_{i=0}^{n} \lambda^i\Psi^{(i)} \right) = \left(\sum_{i=0}^{n} \lambda^i E^{(i)} \right) \left(\sum_{i=0}^{n} \lambda^i\Psi^{(i)} \right). \tag{2.27}$$

Collecting terms with the same power of λ yields a set of n equations:

$$\begin{aligned} H_0\Psi_k^{(0)} &= E_k^{(0)}\Psi_k^{(0)} \\ H_0\Psi_k^{(1)} + V\Psi_k^{(0)} &= E_k^{(0)}\Psi_k^{(1)} + E_k^{(1)}\Psi_k^{(0)}, \\ H_0\Psi_k^{(2)} + V\Psi_k^{(1)} &= E_k^{(0)}\Psi_k^{(2)} + E_k^{(1)}\Psi_k^{(1)} + E_k^{(2)}\Psi_k^{(0)}. \\ &\ldots \end{aligned}$$

Multiplying the LHS by $\Psi_k^{(0)}$ and integrating over the whole space yields the energy expressions:

$$E_k^{(0)} = \left\langle \Psi_k^{(0)} | H_0 | \Psi_k^{(0)} \right\rangle, \tag{2.28}$$

$$E_k^{(1)} = \left\langle \Psi_k^{(0)} | V | \Psi_k^{(0)} \right\rangle, \tag{2.29}$$

$$E_k^{(2)} = \left\langle \Psi_k^{(0)} | V | \Psi_k^{(1)} \right\rangle, \tag{2.30}$$

$$E_k^{(3)} = \left\langle \Psi_k^{(0)} | V | \Psi_k^{(2)} \right\rangle, \tag{2.31}$$

etc. Adding $E_k^{(0)}$ and $E_k^{(1)}$ together, reproduces the Hartree-Fock energy of unperturbed state $\Psi_k^{(0)}$.

The perturbative corrections are introduced through the $E_k^{(2)}$ and higher-order terms. To calculate the first correction, $E_k^{(2)}$, also called the MP2 correction, one introduces the expansion

$$\Psi_k^{(1)} = \sum_i c_i^{(1)} \Psi_i^{(0)}, \tag{2.32}$$

and by putting it into (2.30) one obtains

$$E_k^{(2)} = \frac{1}{4} \sum_{ia} \sum_{jb} \frac{|(ij||ab)|^2}{\epsilon_i + \epsilon_j - \epsilon_a - \epsilon_b} = E_k^{MP2} \tag{2.33}$$

where φ_i and φ_j are the occupied orbitals and φ_a and φ_b are the virtual ones, and ϵ_i, ϵ_j, ϵ_a, and ϵ_b being the corresponding orbital energies.

Spin-Component-Scaled MP2

In case of the MP2 method, the corrections to the unperturbed Ψ_{HF} wave-function are only of second-order. It represents a compromise between accuracy and computational cost. Grimme *et al.* proposed a modification of the MP2 method based on the fact that the correlation energy can be separated into contributions from electron pairs with the same- and the opposite-spin, SS and OS respectively.[5] In standard MP2, both contributions are treated equally

$$E_c^{MP2} = E_c^{MP2,SS} + E_c^{MP2,OS}, \tag{2.34}$$

where E_c^{MP2} corresponds to (2.33). Griemme showed that a simple correction to (2.34) leads to a significant improvement even in cases where MP2 typically fails.[6] The correction is based on a different scaling of the $E_c^{MP2,SS}$ and $E_c^{MP2,OS}$ components. The Spin-Component-Scaled MP2 (SCS-MP2) method is defined as:

$$E_c^{SCS-MP2} = a_{SS} E_c^{MP2,SS} + a_{OS} E_c^{MP2,OS}, \tag{2.35}$$

where a_{SS} and a_{OS} are empirical scaling factors: a_{SS}=1/3 and a_{OS}=6/5.

According to Griemme, in the HF method the SS electron pairs are already correlated, while the OS pairs are not. Low-order MP2 perturbation theory is unable to correct this deficiency. Hence, the non-HF-correlated pair contributions (OS) are scaled-up, while the HF-correlated contributions (SS) are scaled-down in the SCS-MP2 approach. This simple modification yields results close to the very accurate QCISD(T) ones.[6]

Spin-Opposite-Scaled MP2

Based on the success of SCS-MP2 method, Jung *et al.* suggested to neglect the same-spin (SS) contributions completely. By introducing scaling coefficients a_{SS}=0 and a_{OS}=1.3 one defines the Spin-Opposite-Scaled MP2 (SOS-MP2) method. The accuracy of SOS-MP2 method is slightly lower than that of SCS-MP2 but still remains significantly better than that of standard MP2. The major advantage is that the SOS-MP2 method scales with the 4th power of the system size (SCS-MP2 scales with the 5th power) and thus it is applicable to much larger molecules.

2.2.2 Configuration Interaction

The Hartree-Fock SCF procedure recovers a major part of the total energy. The part of energy missing due to the electron-electron correlation, E_c, is nevertheless essential for accurate results. It can be recovered by introducing the Configuration Interaction (CI) expansion. The CI method assumes that the exact N-electron wave-function can be reproduced by a linear combination of Slater determinants

$$\Psi = \sum_{k=0}^{\infty} c_k D_k. \tag{2.36}$$

For practical reasons, the Ψ_{CI} is constructed based on the Hartree-Fock ground-state determinant, by adding determinants corresponding to the singly, doubly, up to N-fold excited states

$$\Psi_{CI} = c_0 D_0 + \sum_{s=0} c_s D_S + \sum_{d=0} c_d D_D + \sum_{t=0} c_t D_T + \ldots + \sum_{n=0} c_n D_N. \tag{2.37}$$

Using the HF determinant as a reference is justified by the fact that it is *the best* possible single-determinant approximation to the exact N-electron wave-function. As a result, the c_0 coefficient of CI expansion (2.37) is typically $\cong 1$ and the determinant D_0 corresponds directly to Ψ_{HF}.

Although E_{corr} is only a very small fraction of the total energy (typically 1 %), a huge number of electronic configurations is required to recover it. The number of configurations included in the CI expansion depends on two factors: the number of electrons in the system, N, and the number of basis functions, M, used in the LCAO expansion. The total number of determinants can be estimated as

$$\text{Number of determinants} \sim \frac{M!}{N!(M-N)!}. \tag{2.38}$$

Typically $M >> N$, and the resulting number is huge. For practical purposes, the CI expansion has to be truncated. The challenging task is to obtain sufficiently accurate CI wave-function with as few expansion terms as possible. A typical approach would be to systematically truncate the expansion after including single, double, triple, or higher excitations from the reference HF state. The excitation refers to assigning an electron to an unoccupied orbital, instead of an occupied one. Although truncating the expansion significantly lowers the computational cost, a large number of terms remains to be computed and the applicability of the CI method is very limited.

In addition, limiting the CI space to a finite number of determinants leads to a size-extensivity problem. The truncated CI methods (CISD, CISDT, *etc.*) do not perform well either in systems of differing size. With increasing size of a molecule, the proportion of the electronic correlation energy contained within a fixed reference space decreases. To compensate for this loss, techniques such as the Davidson correction[7] or the Quadratic CI[8] (QCI) methods has been devised.

For small systems and reasonable basis-sets, the so-called Full-CI method, serves as important benchmark, providing *the exact* solution to the N-electron non-relativistic

Schrödinger equation (within a given basis-set).

Due to their limitations CI methods are being surpassed by the much superior Coupled-Cluster approximation.

2.2.3 Coupled-Cluster

The most important advance over the CI method is known as the Coupled-Cluster Procedure (CC). It resolves the problem of electron-correlation in a non-variational manner. Similarly to the CI methods, the Hartree-Fock ground-state is conveniently chosen as the reference state. An exponential form of the excitation operator T acts on the Ψ_{HF} yielding the Coupled-Cluster wave-function

$$e^T \Psi_{HF} = \Psi_{CC} \tag{2.39}$$

The cluster operator T

$$T = \sum_{i=1}^{N} T_i = T_1 + T_2 + \ldots + T_N, \tag{2.40}$$

generates all the possible N-fold excitations. For instance, the 2-fold excitation operator acting on the reference state Ψ_0

$$T_2 \Psi_0 = \sum_{i>j}^{occ.} \sum_{a>b}^{virt.} t_{ij}^{ab} \Psi_{ij}^{ab} \tag{2.41}$$

generates double excitations from the pairs of occupied states, ij, to the pairs of virtual states ab. The expansion coefficients, t_{ij}^{ab}, also known as the excitation amplitudes, are determined by solving the Coupled-Cluster equations.

For most problems Coupled-Cluster calculations lead to very accurate result, even for relatively short expansions. To illustrate this advantage of CC one can write down the explicit form of the Ψ_{CCSD} wave-function

$$\begin{aligned} \Psi_{CCSD} = e^{(T_1+T_2)}\Psi_0 = \Psi_0 + \sum_{i}^{occ.} \sum_{a}^{virt.} t_i^a \Psi_i^a + \sum_{i>j}^{occ.} \sum_{a>b}^{virt.} t_{ij}^{ab} \Psi_{ij}^{ab} + \\ \frac{1}{2} \sum_{ij}^{occ.} \sum_{ab}^{virt.} t_i^a t_j^b \Psi_{ij}^{ab} + \frac{1}{2} \sum_{i>j}^{occ.} \sum_{k>l}^{occ.} \sum_{a>b}^{virt.} \sum_{c>d}^{virt.} t_{ij}^{ab} t_{kl}^{cd} \Psi_{ijkl}^{abcd} + \ldots \end{aligned} \tag{2.42}$$

From the form of Ψ_{CCSD} in (2.42) it is obvious that apart from the single and double excitations (hence the acronym CCSD), the higher-order excitations are also indirectly included as the so-called disconnected-clusters, with their amplitudes determined by the lower-order excitations. In principle, the CCSD wave-function contains all the possible excitations though the presence of disconnected clusters. This feature of CC is also responsible for the fact that an arbitrarily truncated CC expansion remains size-extensive. This advantageous effects arise from the exponential Ansatz of the CC wave-function.

CCSD(T), the golden standard

By including all the possible N-fold excitations one reaches the Full-CC limit which is consistent with the Full-CI result. As all the advanced post-Hartree-Fock techniques, also the CC method quickly becomes prohibitively expensive with respect to the number of electrons, N, or the basis functions, M. Formally, the CCSD method scales as M^6, while including the triple excitations (CCSDT) leads the the scaling proportional to M^8. It successfully limits the applicability to very small systems.

It is known that out of the higher-order excitations, triples contribute most. Various techniques of estimating the effects of triple excitations have been proposed. Of those, the Coupled-Clusters with singles, doubles and perturbative triples, CCSD(T), emerged as the most robust. This perturbative approach in general slightly overestimates contributions from the triples, but the error is proportional to the effect of ignoring the quadruples and results in a favorable error cancelation. The CCSD(T) method is often called the 'golden standard' of quantum chemistry as it is a reasonable compromise between the less accurate CCSD and the far more expensive CCSDTQ.

2.2.4 Limitations of post-HF methods

Most of the post-Hartree-Fock methods share the same limitations of unfavorable scaling with the increasing number of electrons. The basis-set size dependence is even more pronounced. Hence, in practice, post Hartree-Fock methods typically scale with the fifth or higher power of the number of basis functions. Post-Hartree-Fock techniques are applicable to small or medium systems at best. It is commonly accepted that the application of hierarchically improved methods:

$$HF \rightarrow MP2 \rightarrow CCSD \rightarrow CCSD(T) \rightarrow \ldots \rightarrow FCI,$$

implies application of increasingly larger basis sets (see Table 2.1). In that respect, both the CI and CC-based methods can be interpreted as an effective transformation of the electron-correlation problem into a basis set problem.

Method	HF, SOS-MP2	MP2, SCS-MP2	CCSD	CCSD(T)	CCSDT	CCSDTQ	...	Full-CI
Scaling	M^4	M^5	M^6	M^7	M^8	M^{10}		$M!$

Table 2.1: Scaling of the HF and selected post-HF methods with the number of basis functions, M.

Chapter 3

Density-Functional Theory

The wave-function of an N-electron system, Ψ, depends on $3N$ spatial and N spin coordinates. On contrary, the non-relativistic electronic Hamiltonian contains terms that involve one- and two-electron integrals which involve up to six spatial coordinates only. As such, the wave-function contains more information than is actually needed. An alternative to Ψ, one that involves fewer variables, would thus be desired.

As it occurs, the energy of a system can be expressed in terms of first- and second-order spin-less density matrices. The problem was that there was no convenient prescription on how to calculate these matrices without referring to the wave-function in a first place. Currently, efficient methods to resolve this problem are being developed.[9]

In 1964, Hohenberg and Kohn[10] proved that the non-degenerate ground-state energy, wave-function and all the molecular properties are uniquely determined by the electron probability density, $\rho(r)$, which is the function of only three variables ($r = x, y, z$). The ground-state electronic energy, E_0, can be defined as a functional of the electron density $\rho(r)$:

$$E_0 = E_0\left[\rho(r)\right] = E_0[\rho] \tag{3.1}$$

where the square bracket denotes a functional relation.

3.1 The Hohenberg-Kohn Theorem

The Hohenberg-Kohn theorem states that, if the non-degenerated ground-state electron probability density ρ_0 is known, then it is possible to calculate the ground-state molecular properties from that ρ_0.

Such an assumption implies that the wave-function is redundant and does not have to be known. The theorem is a general statement and as such does not specify how the ground-state energy E_0 can be calculated. In fact, it does not even specify how can the probability density itself be found.

In 1965 Kohn and Sham[11] showed that the exact ground-state energy can be expressed as

$$E_0 = -\frac{1}{2}\sum_{i=1}\left\langle \Psi_i(1)|\nabla^2|\Psi_i(1)\right\rangle - \sum_{\alpha}\int \frac{Z_\alpha \rho(1)}{r_{1\alpha}} dv_1 + \frac{1}{2}\int\int \frac{\rho(1)\rho(2)}{r_{12}} dv_1 dv_2 + E_{xc}[\rho], \tag{3.2}$$

where $\Psi_i(1)$ denotes the Kohn-Sham orbitals and $E_{xc}[\rho]$ is the exchange-correlation functional. The notation $\Psi_i(1)$ and $\rho(1)$ indicate that the Ψ_i and ρ are taken as functions of the spatial coordinates of electron 1. Kohn and Sham showed that the exact ground-state electron density ρ_0:

$$\rho_0 = \sum_{i=1}^{N} |\Psi_i|^2, \tag{3.3}$$

can be found from the Kohn-Sham orbitals. The orbitals itself are determined on the basis of one-electron eigenvalue equations:

$$F_{KS}\Psi_i(1) = \epsilon_{i,KS}\Psi_i(1). \tag{3.4}$$

Here the Kohn-Sham operator F_{KS} is given as

$$F_{KS} = -\frac{1}{2}\nabla_1^2 - \sum_{\alpha}\frac{Z_\alpha}{r_{1\alpha}} + \sum_{j=1} J_j(1) + V_{xc}(1), \tag{3.5}$$

with the Coulomb operator $J_j(1)$ defined as

$$J_j(1) = \int |\Psi_j(2)|^2 \frac{1}{r_{12}} dv_2, \tag{3.6}$$

and the exchange-correlation potential

$$V_{xc} = \frac{\delta}{\delta\rho} E_{xc}[\rho]. \tag{3.7}$$

The Kohn-Sham operator F_{KS} is similar to the Fock operator (2.11). In the DFT formalism the exchange operators are replaced by V_{xc}, which handles the effects of exchange and correlation simultaneously.

3.2 Exchange-Correlation functional

The DFT method is in principle an exact, yet it is impossible to solve the N-electron equations in exact manner. The problem resides in the exchange-correlation functional. Because the exact form of $E_{xc}[\rho]$ for molecules remains unknown, approximations have to be introduced. As of this moment, scores of approximate functionals are available.

The hierarchy of density functional approximations is typically pictured as the so-called 'Jacob's ladder'. The quality of a functional is expected to increase as one gets higher up on the ladder. The first rung is the Local-Density Approximation (LDA), exact for the uniform electron gas and often quite accurate for solids, particularly metals. The

second rung is the Generalized-Gradient Approximation (GGA), third is meta-GGA, *etc.* Nonetheless, at a given level of approximation it is difficult to choose *the best* functional without referring to previous calculations or experimental references. The systematic improvement in accuracy is thus limited to factors such as the basis-set size.

3.2.1 Local-Density approximation

If $\rho(r)$ varies slowly with position, the $E_{xc}[\rho(r)]$ may be expressed as:

$$E_{xc}[\rho(r)] = \int \rho(r)\epsilon_{xc}[\rho(r)]dr \tag{3.8}$$

where $\epsilon_{xc}[\rho(r)]$ is the exchange-correlation energy per electron for the homogeneous electron gas with electron density $\rho(r)$. The homogeneous electron gas is a hypothetical infinite-volume system consisting of an infinite number of electrons. It is assumed that the distribution of electron density in such system is uniform and the number of electrons per unit volume has a non-zero value of $\rho(r)$.

Applying the functional (3.8) yields the Local-Density Approximation (LDA). In a molecule the positive charge is localized at the nuclei, and the electron distribution varies rapidly with the distance from a given nucleus. Molecular LDA calculations show only fair agreement with experiment. Certain improvement is obtained by introducing different K-S orbitals, and thus densities, for electrons with different spins. The extension is called Local Spin-Density Approximation (LSDA).

The 'high-accuracy' LSDA calculations performed for selected diatomic molecules[12] found average absolute errors of 2 pm in R_e, 1.0 eV in D_e and 3.3 % in vibrational frequencies. While the distances are reproduced with reasonable accuracy, the dissociation energies are poor. It is a typical behavior of LDA methods.

3.2.2 GGA and meta-GGA approximations

Since its introduction, the LDA was particularly popular in the field of solid-state physics, but it was the generalized-gradient approximation (GGA) that made DFT popular in quantum chemistry as well. The key improvement were improved binding energies. GGA expresses the exchange-correlation energy in terms of the densities, but also their local gradients:

$$E_{xc}[\rho(r)] = \int \rho(r)\epsilon_{xc}[\rho(r), \nabla\rho(r)]dr. \tag{3.9}$$

The $\epsilon_{xc}[\rho(r), \nabla\rho(r)]$ is not uniquely defined for GGA resulting in many different flavors of GGA-based methods. Even more advanced are the so-called meta-GGA functions. These functionals include additional terms that depend on the Laplacian of the density.

Introduction of explicit gradient dependence improves the quality of DFT calculations and yields better results for both solids and gas-phase species.

PBE functional

The PBE functional Perdew, Burke and Ernzerhof[13] is constructed in such a way that all the essential features of LDA are preserved. It combines them with the energetically

most important features of gradient-corrected nonlocality. The PBE functional in a non-empirical functional, whose all parameters are derived from theory.

3.2.3 Hybrid functionals

Hybrid functionals are a class of functionals where the exchange-correlation term incorporates a certain portion of exact exchange from Hartree-Fock theory. A hybrid functional is usually constructed as a linear combination of the Hartree-Fock exact exchange functional (E_x^{HF}) and several other exchange and correlation density functionals. The parameters determining the weight of each individual functional are specified by fitting the results to reliable data. The concept of hybridizing the Hartree-Fock method with Density Functional Theory was first introduced in 1993 by Becke.

B3LYP functional

Among the many available hybrid functionals, the B3LYP exchange-correlation functional is the most popular among chemists. It is constructed in the following way:

$$E_{xc}^{\mathrm{B3LYP}} = E_{xc}^{\mathrm{LDA}} + a_0(E_x^{\mathrm{HF}} - E_x^{\mathrm{LDA}}) + a_x(E_x^{\mathrm{GGA}} - E_x^{\mathrm{LDA}}) + a_c(E_c^{\mathrm{GGA}} - E_c^{\mathrm{LDA}}),$$

where a_0=0.20, a_x=0.72, and a_c=0.81 are three empirical parameters determined by fitting the predicted values to a set of experimentally known atomization energies, ionization potentials, proton affinities, and total atomic energies. The E_x^{GGA} and E_c^{GGA} terms are based on the generalized gradient approximation: the Becke (B88) exchange functional[14] and the correlation functional of Lee, Yang and Parr (LYP).[15] The remaining E_c^{LDA} is the Vosko, Wilk and Nusair (VWN) LDA functional.[16]

TPSS and TPSSh functionals

In 2008 Tao *et al.*[17] proposed a new non-empirical meta-GGA exchange-correlation functional, TPSS. Construction of the functional is based on the Perdew-Kurth-Zupan-Blaha (PKZB) meta-GGA functional.[18] As its predecessor the TPSS functional is designed to yield correct exchange and correlation energies through second-order in ∇ for a slowly-varying density (solids) and the correct correlation energy for any one-electron density (molecules).[17]

Initial tests[17] show that the TPSS gives excellent results for a wide range of systems. In particular, it correctly describes bond lengths in molecules, hydrogen-bonded complexes and ionic solids. The practical advantage of TPSS functional is that it does not incorporate HF exchange. This feature is particularly important for solid-state calculations where the exact HF exchange is usually inaccessible due to the exceedingly high computational cost.

Hybridizing the exact HF exchange with the non-empirical TPSS functional yields a hybrid. The TPSSh exchange-correlation functional is defined as

$$E_{xc}^{TPSSh} = a_0 E_x^{HF} + (1 - a_0)E_x^{TPSS} + E_c^{TPSS}$$

where the empirical parameter a_0=0.10 is determined by minimizing the mean absolute deviation in the enthalpy of formation of 223 molecules. The small value of a_0 (smaller

by about 20 % than for a typical hybrid functionals) indicates that the TPSSh functional better approximate the still unknown exact exchange-correlation functional than other standard hybrid functionals.[19]

3.2.4 Double-hybrid functionals

An example on a new generation of the so-called double-hybrid functional is B2PLYP. The functional is constructed in such way that the explicit orbital correlation occurs. As a result, in addition to a non-local exchange contribution, a non-local perturbation correction for the correlation part is also introduced. The idea is rooted in the $ab\text{-}initio$ Kohn-Sham perturbation theory (KS-PT2) of Görling and Levy.[20,21]

First, one defines a standard hybrid-functional within the GGA approximation. Then, self-consistent Kohn-Sham calculations are performed. The resulting solutions, the KS orbitals and the eigenvalues, are used as input in the MP2-type calculations. The resulting KS-PT2 correction replaces part of the semi-local GGA correlation. The non-local perturbation correction to the correlation contribution is given by

$$E_c^{KS-PT2} = \frac{1}{4}\sum_{ia}\sum_{jb}\frac{|(ij||ab)|^2}{\epsilon_i + \epsilon_j - \epsilon_a - \epsilon_b}$$

The mixing is described by two empirical parameters a_x and a_c in the following manner:

$$E_{xc}^{B2PLYP} = (1-a_x)E_x^{GGA} + a_x E_x^{HF} + (1-a_c)E_c^{GGA} + a_c E_c^{KS-PT2} \qquad (3.10)$$

where E_x^{GGA} and E_c^{GGA} are the energies of a chosen exchange and correlation functionals, E_x^{HF} is the exact Hartree-Fock exchange of the occupied Kohn-Sham orbitals, and E_c^{KS-PT2} is a perturbation correction term based on the KS orbitals.

The method is self-consistent only with respect to the first three terms of (3.10). For B2PLYP functional, the B88 exchange[14] and LYP correlation[15] are used with the parameters $a_x = 0.53$ and $a_c = 0.27$. According to Schwabe *et al.*[22] the only known basic deficiency of the B2PLYP approach is due to Self-Interaction Error (SIE). Thanks to the relatively large fraction of the SIE-free HF exchange, these affects are alleviated in B2PLYP. In addition, unwanted effects of increased Fock exchange, such as the reduced account of static correlation, are damped or eliminated by the KS-PT2 term.[5]

3.3 Limitations of DFT

Although most of the functionals are not defined in the strict $ab\text{-}initio$ manner, the inclusion of a small portion of HF exchange and the efficient empirical parameterization yield surprisingly good results for many molecular properties. The results are often comparable with computationally much more expensive wave-function based methods, such as MP2 or even Coupled-Cluster methods. Nevertheless, most of the commonly applied exchange-correlation functionals share the same negative feature of not being able to describe dispersion interactions in a reliable manner.[23]

Chapter 4

Solid-state implementations

When dealing with solids, the question arises, how can one handle the infinite number of interacting electrons moving in the static field of an infinite number of ions? What is the shape of wave-function that describes such system?

In a regular crystal, ions are arranged with regular periodicity. The potential V, felt by the electrons,

$$V(r) = V(r + R), \tag{4.1}$$

is thus periodic. The periodicity can be employed to simplify the calculations. Bloch's theorem exploits (4.1) to reduce the infinite number of one-electron wave-functions to the number of electrons in a unit cell.

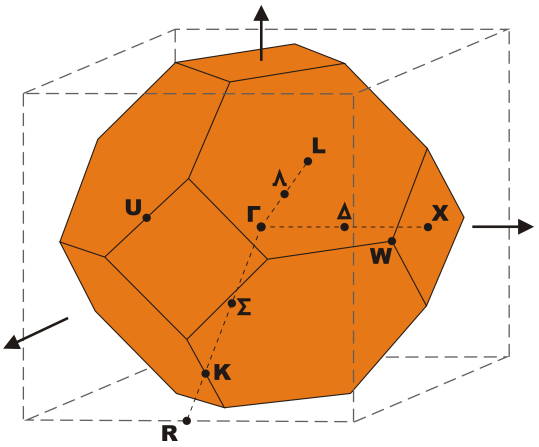

Figure 4.1: The First Brillouin Zone of face-centered cubic (fcc) lattice with labels for high symmetry critical points.

4.1 Bloch's theorem

Bloch's wave-function describes a particle moving in a periodic potential. It is defined as a product of two contributions, an exponential plane-wave envelope function and a periodic function:

$$\Psi_{n,k}(r) = e^{ikr}\Phi_{n,k}(r) \tag{4.2}$$

The $\Psi_{n,k}$ product exhibits the same periodicity,

$$\Psi_{n,k}(r) = \Psi_{n,k}(r + R), \tag{4.3}$$

as the potential. The corresponding one-particle energy $E_n(k)$=$E_n(k + K)$ is also periodic. The energy associated with index n varies continuously with wave-vector k. For that reason it is more appropriate to speak of energy bands n instead of discrete energy levels.

According to Bloch's theorem all the distinct values of $E_n(k)$ occur within the so-called First Brillouin Zone of the reciprocal lattice. The energy solutions, $bands$, are separated in energy by a finite spacing at each k. If the separation extends over all wave-vectors, it is called a $band\ gap$.

Within the independent electron approximation, all properties of a periodic system can be calculated from the band structure and the associated Bloch wave-function. Application of Bloch's theorem maps the problem of infinite number of electrons onto the problem of expressing the wave-function in terms of an infinite number of reciprocal space vectors within the FBZ. This problem is dealt with by sampling the Brillouin zone at finite sets of k-points.

4.1.1 First Brillouin Zone

Brillouin zones characterize crystal structures in momentum space.[24] The First Brillouin Zone (FBZ) is defined as the Wigner-Seitz cell in that reciprocal space. The Wigner-Seitz cell itself is defined as the smallest polyhedron enclosed by the perpendicular bisectors of the nearest neighbors to a lattice point. Higher-order Brillouin zones can be defined as next-smallest polyhedra enclosed by bisecting planes.

For an extended periodic system, the uniquely defined FBZ is most important. It completely characterizes the $whole$ crystal. If one wants to consider all the possible electronic states in the infinite crystal, one needs to investigate the FBZ only. This follows directly from Bloch's theorem for the wave-function.

Within the First Brillouin Zone, points of high symmetry - called critical points or k-points - are particularly interesting (see Table 4.1). Of them, the Γ-point identifies the center of FBZ, while other points can identify for example ends of FBZ in different directions in k-space. Different types of critical points can be defined for different lattice symmetries. An example on face-centered cubic (fcc) lattice is shown in Fig. 4.1.

4.1.2 k-points

The First Brillouin Zone consists of a continuous set of k-points, throughout a region of reciprocal space (k-space). The occupied states at each k-point contribute to the electronic potential of bulk solid. There exist an infinite number of k-points at which the wave-functions must be calculated. Those k-points that are very close together are almost identical. It is thus possible to represent the electronic wave-functions over a small region of reciprocal space at just a single k-point. This approximation allows the electronic potential to be calculated at a finite grid of points and yield the total energy

Symbol	Description
Γ	Center of the Brillouin zone
	Simple cubic (sc)
M	Center of an edge
R	Corner point
X	Center of a face
	Face-centered cubic (fcc)
K	Middle of an edge joining two hexagonal faces
L	Center of a hexagonal face
U	Middle of an edge joining a hexagonal and a square face
W	Corner point
X	Center of a square face
	Body-centered cubic (bcc)
H	Corner point joining four edges
N	Center of a face
P	Corner point joining three edges
	Hexagonal (hex)
A	Center of a hexagonal face
H	Corner point
K	Middle of an edge joining two rectangular faces
L	Middle of an edge joining a hexagonal and a rectangular face
M	Center of a rectangular face

Table 4.1: Labeling of the most important First Brillouin Zone critical points for selected lattice symmetries. For the fcc example, see Figure 4.1

of a solid. The error due the k-space sampling can be made arbitrarily small by choosing a sufficiently dense set of k-points.

The number of k-points necessary for a reliable calculation depends on the expected accuracy and on the nature of the system. Metallic systems require an order-of-magnitude more k-points than semiconductors and insulators. Also, different methods converge with different speeds, which are highly dependent on the extent of the sampled k-space.

Typically the error due to the insufficient number of k-point considered is not transferable to different lattice types (fcc, bcc, *etc.*) or with respect to the size of a unit cell. For small cells it is necessary to include more k-points while for large super-cells already the Γ-point corresponds to many k-points in the First Brillouin Zone. Therefore the absolute convergence with respect to the number of k-points must be studied individually for each case.

By sampling the electronic wave-functions at specially designed sets of k-points, very accurate approximations to the electronic potential can be obtained. The two most common methods are those of Chadi and Cohen,[25] and Monkhorst and Pack.[26]

4.1.3 Sampling grids

In practical solid-state calculations one needs to use a finite number of k-points to sample the FBZ. Choosing a finite grid is acceptable as long as the orbitals vary smoothly with k. In most of the cases a grid of Monkhorst and Pack[26] is applied, particularly because it is unbiased by the choice of the k-points in the FBZ.

Monkhorst-Pack grid is a rectangular grid, spaced evenly throughout the FBZ. Similarly to the cut-off energy, the choice of the grid size depends on the system. The appropriate size is typically established by means of a convergence test. A general rule states that the larger the dimensions of the grid, the finer and more accurate will be the sampling.

4.1.4 Band Structure

Solving the Kohn-Sham equations yields $\frac{N}{2}$ orbitals for each of the k-points used in sampling the FBZ. The resulting KS orbitals are solutions of a single-particle Schrödinger-like equation with the local Kohn-Sham potential. Using these solutions one can solve the equations for k-points other than those in the original k-point set. Such complete set of eigenvalues for each k-point forms the $band\ structure$. In many cases it is a good approximation to the true band structure of the interacting system.

4.1.5 Density of States

The $Density\ of\ States$ (DOS) describes the number of states that can be occupied in a given system at each energy level. The zero value of DOS means that no states can be occupied at the corresponding energy level. The product of the DOS and the $probability\ distribution$ gives the number of occupied states at a given energy per unit volume. The DOS analysis provides important information on physical properties of solids, such as conductivity and its type.

Chapter 5

Approximations and methods

5.1 Born-Oppenheimer approximation

In a system composed of electrons and atomic nuclei, the momentum transfer between interacting particles is typically very small, due to a large difference in masses. Assuming that the forces acting on the particles are comparable and that their momenta are similar, the nuclear velocities must be much smaller than the velocities of electrons. Therefore it is not unreasonable to separate the electronic and nuclear motion. Such an approach is called the Born-Oppenheimer (BO) approximation.[27]

By applying the Born-Oppenheimer approximation, the electronic eigenvalue problem is solved for the potential of nuclei at fixed locations. Once the ground state electronic configuration is known, the nuclear degrees of freedom could also be solved giving rise to nuclear motion. Varying the nuclear positions maps out the potential energy surface (PES) of the ground state.

The typical errors due to the Born-Oppenheimer approximation are small for the electronic ground state and only slightly larger for excited states. The errors are usually much smaller than those resulting from most other approximations used to solve the N-electron Schrödinger equation (i.e. approximate treatment of electronic correlation, relativistic effects, basis sets, $etc.$). Hence the separation of nuclear and electronic variables leads to a significant reduction in computational cost. Had it not been for Born-Oppenheimer approximation, computational quantum chemistry might not be there in its current form. For small systems, calculations are now reported that treat electronic and nuclear motion on equal footing.[28,29]

Born-Oppenheimer Diagonal Correction: In a perturbative analysis of the BO approximation, the first-order correction to the electronic energy due to the nuclear motion is the Born-Oppenheimer diagonal correction (BODC):

$$E_{BODC} = \langle \Psi(r;R) | T_N | \Psi(r;R) \rangle \tag{5.1}$$

where $\Psi(r,R)$ is an arbitrary electronic state and T_N is the kinetic energy operator of the nuclei. Valeev and Sherrill estimated the BODC and its convergence toward the $ab\text{-}initio$ limit using CI wave-functions. They found that although the absolute value is actually difficult to converge with respect to the basis-set size, it is actually properly estimated already at the Hartree-Fock level of theory.[30]

5.2 Harmonic approximation

The electronic energy, E_{el}, depends on the distances between nuclei. For a diatomic molecule, the shape of $E_{el} = E(R)$ may be approximated by a Morse function $U = U(R)$, see Fig. 5.2. The Morse potential explicitly includes effects of bond breaking, i.e. it can properly describe dissociation processes and the existence of unbound states. Despite obvious advantages, the analytical solution is complicated and simplifications are needed. The commonly applied technique introduces the harmonic potential $U'(R)$ which is a quadratic approximation to $E(R)$. If the origin of potential $U'(R)$ is placed so that it coincides with the minimum point, R_e, of the Morse potential $U(R)$, than the lower part of $U'(R)$ will practically coincide with the approximate potential-energy curve of a harmonic oscillator with the approximate force constant k. Therefore, the vibrational energy levels can be reasonably approximated by the harmonic oscillator vibrational energy levels

$$E_{vib} \approx (\omega + \frac{1}{2}h\nu_e), \tag{5.2}$$

$$\nu_e = \frac{1}{2\pi}\left(\frac{k}{\mu}\right)^{\frac{1}{2}}, \qquad \mu = \frac{m_1 m_2}{m_1 + m_2}, \tag{5.3}$$

where ν_e is the harmonic vibrational frequency, μ is the reduced mass, and the harmonic force constant k is

$$k = \frac{d^2U'(R)}{dR^2} \approx \left[\frac{d^2U(R)}{dR^2}\right]_{R=R_e}. \tag{5.4}$$

The error introduced by a harmonic approximation grows for higher values of ω. Therefore, the harmonic approximation is best suited for the description of the lower part of the vibrational spectrum (see Fig 5.2). In the present work anharmonic corrections were considered in Paper V.

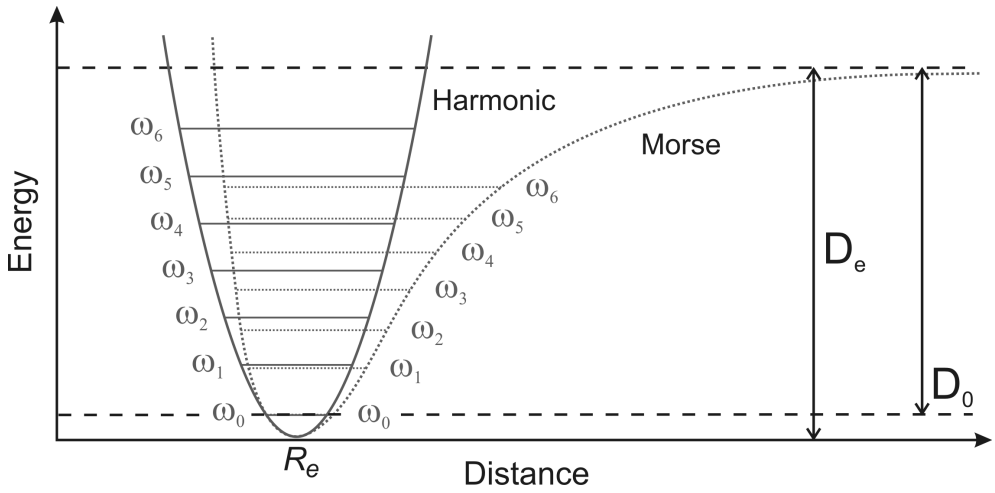

Figure 5.1: A qualitative comparison of the harmonic and the Morse potential energy curves.

5.3 Basis sets

Most quantum chemical calculations are performed within a finite set of M basis functions. The one-electron wave-functions are expanded as linear combinations of those basis functions

$$\Psi = \sum_{i}^{M<\infty} c_i \chi_i \rightarrow [c_1, c_2, ..., c_M]. \tag{5.5}$$

One typically has to choose between more complete, and therefore computationally more expensive basis sets, and smaller, less accurate but cheaper basis sets. If the basis were expanded towards a complete set, the calculations would approach the exact result. In reality, a balance has to be found.

Different molecular calculations typically require different basis sets.

5.3.1 Basis functions

The first type of basis sets is constructed from Slater-type orbitals (STO). The functional form of an STO is

$$\chi_{\zeta,n,l,m}(r,\theta,\varphi) = NY_{l,m}(\theta,\varphi)r^{n-1}e^{-\zeta r}. \tag{5.6}$$

Here N is a normalization coefficient and $Y_{l,m}(\theta,\varphi)$ are spherical harmonic functions.

In general, the STOs are not solutions to the atomic Schrödinger equation. However the behavior near the nucleus and towards infinity have the correct form. The radial part lacks any nodal structure, but it can be recovered through linear combinations. Apart from the ADF code, Slater-type basis sets are typically used in high-accuracy calculations of atomic or diatomic systems only.

An alternative is provided by the Gaussian-type orbitals (GTO). The GTOs are defined as

$$\chi_{\zeta,n,l,m}(r,\theta,\varphi) = NY_{l,m}(\theta,\varphi)r^{2n-2-l}e^{-\alpha r^2}. \tag{5.7}$$

The r^2 in the exponent suggests that the GTO are inferior to the STOs. By definition, Gaussian-type functions lack the so-called cusp at the nucleus. At the nucleus, the first derivative is equal to zero, while in reality the derivative should approach a constant. More quantitatively, the Kato cusp condition states that

$$\lim_{r\to 0}\left\langle \frac{\partial\Psi}{\partial r}\right\rangle = -Z\Psi(r=0). \tag{5.8}$$

As a result, the description of the wave function, close to the nucleus, provided by the GTO, is problematic. Moreover, the part further away from the nucleus is also described inaccurately, because the GTO falls off more rapidly as compared to the analogous STO. Both problems can be minimized to a high degree by introducing more basis functions in the linear combination.

In principle, both Slater and Gaussian type basis functions can be used for the construction of a basis-set. Due to the nature of GTO, the number of required basis

functions is larger. A rough estimate indicates that approximately three times more GTOs than STOs are needed to achieve a similar level of accuracy. Although GTOs are theoretically inferior to STOs, the much cheaper two-electron integrals make them competitive.

5.3.2 Basis set size

The simplest, *minimal basis* has only one effective Slater function per atomic orbital (such as 1s). Doubling the number of basis functions results in the Double-Zeta (DZ) basis set. In the case of hydrogen, such a set contains two s-functions with different exponents. Increasing the number of basis functions provides flexibility and allows for better description of electron distribution.

In most chemical applications, a systematic increase (doubling, tripling, *etc.*) of the number of basis functions in the core and valence space does not provide equal increase in accuracy, while it does increase the computational requirements. For instance, increasing the number of functions with large exponents will improve the description of the core region, but it will have a minor effect on the valence space responsible for bonding. Since the energetically deep lying, or the *core electrons*, are essentially independent of the chemical environment, they can be accurately described with fewer basis functions.

5.3.3 Contraction schemes

The wave-function is not uniform. Different parts of Ψ require different treatment. The core electrons located close to the nucleus, account for much larger fraction of the total energy than the valence electrons. Variational optimization of a basis set with respect to the total energy would favor the core electrons leaving the valence space too poor in basis functions. For chemical purposes one would prefer the opposite. To achieve this, typically one of the following contraction schemes is applied.

Segmented contraction: A set of M primitive Gaussian-type orbitals (pGTO) is first divided into subsets (s-, p-, d-, *etc.*). These secondary subsets are then contracted into a set of gaussian type orbitals (cGTO) with predetermined coefficients c_i

$$\bar{\chi}_1(cGTO) = \sum_{i=a}^{b} c_i \chi_i(pGTO),$$

In segmented contraction scheme, a given pGTO is usually used only once for each type of cGTO.

General contraction: The basis set is not divided into secondary subsets. Instead the scheme allows for construction of contracted gaussian type orbitals (cGTO) using all available primitives within the same angular momentum space. General contraction scheme provides additional flexibility but it is also computationally more expensive. The most popular basis sets that rely on a general contraction scheme are the family of correlation-consistent basis sets.

5.3.4 Split-valence basis sets

For an accurate bonding analysis, the valence space must be described particularly well. In the *split-valence* (SV) basis set the functional space is divided into the core and valence spaces. The doubling (tripling, *etc.*) of basis function applies to the valence space only. Such an approach results in basis sets that are flexible enough for an accurate bonding description but remain computationally affordable even for larger sets.

Within the valence space, higher angular momentum functions are usually important and must be eventually added to the basis set. For main-group elements a linear combination of s-, p- and d-functions is insufficient for proper description. Introduction of l-functions (l=f, g, h, *etc.*) provides additional degrees of freedom in the angular space. The f-function polarizes the d-function, just as the d-function polarizes the p-function.

For a single-determinant wave-function (i.e. Ψ_{HF}), one set of polarization functions is usually sufficient for the accurate description of charge polarization effects. For post-HF methods that treat electron correlation explicitly, the introduction of additional basis functions is essential. Electron correlation lowers the HF energy by letting the electrons avoid each other. Several distinct types of correlation can be identified. In the case of radial, 'in-out' correlation, one electron is much closer to the nucleus than the other. For proper description, additional basis functions with substantially different exponents are needed. In the case of angular correlation, electrons try to avoid each other by occupying opposite sides of the nucleus. For this type of correlation, basis functions with different angular momenta are required. Both types of correlation are of the same order of magnitude.

Typically, exponents of polarizations functions are similar to the exponents of other valence basis functions. It corresponds to the fact, that mainly the valence-electrons are correlated and the core-electrons are left unperturbed. For very accurate calculations, also core and core-valence polarization functions should be included.

5.3.5 Correlation-consistent basis sets

The correlation-consistent (cc) basis sets are a class of basis sets specially designed for a systematic, high-accuracy recovery of the correlation energy. They include polarization functions which contribute similar amounts of correlation energy at the same stage, independently of the type. For instance, if the p-space is correlated, the correlation energy correction resulting from introducing the first d-function lowers the energy significantly. Introduction of an additional d-function will also lead to energy lowering, but a similar correction would result from introducing one f-function. Hence, both should be included in the same step of basis set enlargement. In order to maintain consistent increase in quality, polarization functions are added in the order: 1d, 2d1f, 3d2f1g, 4d3f2g1h, *etc.* To maintain a balance between the number of s- and p-functions and the higher-angular-momentum polarization functions, the number of s- and p-functions must also increase in a consistent way.

A large number of correlation-consistent basis sets is available. The most common are the cc-pVnZ (n = D, T, Q, 5, ...). The acronym refers to 'correlation-consistent polarized valence n zeta'. Several examples are illustrated in Table 5.1.

The scheme used in construction of cc basis sets leads to a rapid increase of the total number of basis functions. This is particulary disadvantageous in wave-function based

Basis	s- and p-type pGTOs	polarization pGTOs
cc-pVDZ	9s, 4p	1d
cc-pVTZ	10s, 5p	2d, 1f,
cc-pVQZ	12s, 6p	3d, 2f, 1g
cc-pV5Z	14s, 9p	4d, 3f, 2g, 1h
cc-pV6Z	16s, 10p	5d, 4f, 3g, 2h, 1i

Table 5.1: Selected correlation-consistent basis sets in terms of primitive gaussian type orbitals (pGTO).

theories, where the computation cost rises as M^a, a$\geq$4 with respect to the number of basis functions.

5.3.6 Plane-wave basis sets

In addition to localized basis sets, plane-wave (PW) basis sets can also be used in quantum chemical simulations. Typically the number of plane-wave-functions is limited by a cut-off energy. Plane-wave basis sets are most suitable for calculations involving periodic boundary conditions. Certain integrals and operations are easier to implement and carry out.

An important advantage of any plane-wave basis is the systematic convergence towards the exact wave-function with respect to the cut-off energy. All functions in the PW basis set are mutually orthogonal, and the basis set does not exhibit a basis set superposition error (see Section 5.5). However, when the volume of the cell changes, the number of plane-wave components varies discontinuously and corrections should be introduced to compensate.[31]

Plane-waves are less well suited for gas-phase calculations. They are typically used, in combination with pseudopotentials (see Section 5.6), because they have difficulties describing the wiggles on the wave-function close to the nucleus.

5.4 Basis set incompleteness error

Typical calculations focus on the valence region of the wave-function. Most of the basis sets are constructed in such way that the valence space is somewhat richer in basis functions, typically due to lower contraction. In the majority of cases, correlation of the valence electrons is the most important. The core electrons are kept 'frozen', they are not correlated.

The valence space of many modern basis sets can approach completeness and the core-core and core-valence effects start to be non-negligible.[32,33,34] Studies on reference molecules shows that core-electron correlation effects should be considered upon enlarging the basis set to quintuple-zeta quality.[35]

Application of even larger, 6Z basis sets can still recover a minor fraction of the correlation energy, which for lighter elements is typically comparable to the magnitude of relativistic effects.[36] The rather uncommon 7Z and 8Z basis sets would lead to improvement in correlation energy comparable in size to the error introduced by the

Born-Oppenheimer approximation.

For light elements, 6Z quality basis sets are typically large enough to reproduce the non-relativistic limit. For calculations involving heavier elements other subtle effects, such as spin-orbit interactions, are typically as important as the basis sets size.

5.5 Basis set superposition error

Using a complete basis set is impossible. The number of basis functions must be limited to some finite number, M, with some highest $l_{\max}$.

Most calculations employ atom-centered bases with relatively few basis functions. Unfortunately, this technique is sensitive to the relative positions of nuclei. When comparing two significantly different geometries, application of the nuclear-fixed basis sets leads to inconsistencies. For a given geometry the electron density around a nucleus A may be described by functions centered on nucleus B which was not present in the vicinity of A at the other geometry. In such situations, the finite nature of the basis set may considerably affect the calculations, particularly if weak interactions are involved. This effect is known as the basis-set superposition error (BSSE) and is a direct result of the basis set incompleteness.

The BSSE vanishes only for a complete basis set. A brute-force solution to diminish the BSSE is ruled out by the cost. In addition, adding a large number of basis functions can also quickly lead to numerical issues such as basis set linear dependence.

The most-commonly applied approximate way of correcting for the BSSE is the counterpoise (CP) correction.

For a dimer, the uncorrected interaction energy, E_{int}, is calculated as

$$\Delta E_{int} = E(AB)^*_{ab} - E(A)_a - E(B)_b \tag{5.9}$$

where the monomers A and B are described with basis sets a and b, and the dimer AB is described by combined basis set ab. The asterisk indicates a dimer geometry. To estimate how much of ΔE_{int} is due to the BSSE, four additional numbers are needed: a) the energies $E(A)^*_a$ and $E(B)^*_b$ of monomer A and B, with their corresponding basis sets a and b, calculated at geometries they have in the dimer, b) the energies $E(A)^*_{ab}$ and $E(B)^*_{ab}$ of both monomers at their dimer geometries, calculated with the combined ab basis set. The CP correction is then defined as

$$\Delta_{CP} = E(A)^*_{ab} + E(B)^*_{ab} - E(A)^*_a - E(B)^*_b \tag{5.10}$$

thus the CP-corrected interaction energy, E^{CP}_{int} is

$$E^{CP}_{int} = \Delta E_{int} - \Delta_{CP}. \tag{5.11}$$

The counterpoise-corrected interaction energy typically approaches the basis set limit much faster than the uncorrected value.

5.6 Pseudopotentials

Chemists are typically interested in the bonding which is determined by the valence region of the atoms. For light elements the core region includes few electrons and is usually of minor direct importance. On contrary, for heavy elements the core include dozens of electrons. The speeds of electrons moving in the vicinity of highly charged nuclei approach the speed of light. The relativistic effects are thus very pronounced. Although core electrons are not directly involved in bonding, changes in the deep-lying orbitals affect the whole electronic structure.

Because the deep-core part of a heavy atom remains practically inert during any chemical reaction, the explicit treatment of the inner-most electrons can be reproduced by applying pseudopotentials.

The pseudopotential (PP) technique models the core-potential with a Gaussian expansion

$$U_{PP}(r) = \sum_i a_i r^{n_i} e^{-\alpha_i r^2} \tag{5.12}$$

where parameters a_i, n_i and α_i are determined by fitting to numerical data obtained from high-precision all-electron calculations employing methods such as Multi Reference Dirac-Hartree-Fock. This approach simultaneously eliminates large number of inner electrons, and their basis functions from the calculations. In addition, pseudopotentials emulate the relativistic effects at scalar or spin-orbit level at no additional cost.

Application of pseudopotentials fitted to the high-precision all-electron non-relativistic results provides convenient insight into these two distinct realms.

Pseudopotentials: solids

Although plane-waves are the natural choice for basis functions for the periodic calculations, they are poorly suited for describing the core-part of a wave-function. A large number of functions is typically needed to accurately describe the rapidly oscillating electronic wave-function close to the nucleus. In principle, it is possible to use Bloch's functions with sufficiently high cut-off energies to find the accurate solutions to the Kohn-Sham equations for infinite crystalline systems.

As in the case of discrete molecules, most physical and chemical properties of extended systems depend mostly on the valence electrons. The pseudopotential techniques are thus commonly applied. The pseudopotentials for solids are typically constructed in such a way that they have no radial nodes in the core region of the wave-function. The wave-function and the pseudopotential are identical to the all-electron wave-function and potential outside a certain cut-off radius. It significantly lowers the computational cost and allows for the inclusion of relativistic and other effects.

5.7 Resolution of Identity

To decrease the computational cost of calculations it is advantageous to separate the Coulomb and exchange contributions to the total energy.

One can expand the density $\rho(r)$ in an $auxiliary\ basis\ set$

$$\rho(r) = \tilde{\rho}(r) = \sum_{\alpha} c_\alpha \alpha(r), \tag{5.13}$$

and introduce the Resolution of the Identity (RI)

$$\langle\rho|\rho\rangle \geq \langle\tilde{\rho}|\tilde{\rho}\rangle = \sum_{\alpha,\beta} \langle\rho|\alpha\rangle \langle\alpha|\beta\rangle^{-1} \langle\beta|\rho\rangle, \tag{5.14}$$

where

$$\sum_{\alpha,\beta} |\alpha\rangle \langle\alpha|\beta\rangle^{-1} \langle\beta| \approx 1. \tag{5.15}$$

Using (5.15), an approximate form of the Coulomb operator (2.12), defined in the Coulomb metric[37]

$$\langle x|y\rangle =: \int x(1)\frac{1}{r_{12}}y(2)d\tau$$

can be written as

$$\tilde{J} = \frac{1}{2}\sum_{\alpha,\beta} \langle\rho|\alpha\rangle \langle\alpha|\beta\rangle^{-1} \langle\beta|\rho\rangle = \sum_{a,b,c,d,\alpha,\beta} D_{ab} \langle ab|\alpha\rangle \langle\alpha|\beta\rangle^{-1} \langle\beta|cd\rangle D_{cd}. \tag{5.16}$$

The RI approximation is based on the expansion of products of virtual and occupied orbitals in the $auxiliary\ basis\ set$. In (5.16), a four-center integral is replaced by three- and two-center integrals. Since such integrals are analytically solvable, the RI approximation provides significant computational savings with a minimal loss of accuracy. The RI approximation for the Coulomb energy (RI-J) drastically decreases computational cost of large-scale calculations, resulting in the asymptotic scaling proportional to N^2.

Chapter 6

The relativistic framework

In 1928 Dirac introduced a wave-equation that was consistent with both the principles of quantum mechanics and the special relativistic requirement of Lorentz covariance

$$H_D \Psi_D = E_D \Psi_D \tag{6.1}$$

Although equation (6.1) seems identical in form to the Schrödinger equation (1.3), it provides significant improvement in the description of a particles with spin $s = \frac{1}{2}$.

6.1 Dirac equation

Dirac showed that in the absence of external electromagnetic field, the Hamiltonian describing an energy spectrum of a free electron is

$$H_D = c\boldsymbol{\alpha} \cdot \boldsymbol{p} + \boldsymbol{\beta} m_0 c^2 \tag{6.2}$$

where m_0 is the mass of electron in rest, $\boldsymbol{p}$ is the angular momentum operator, and c the speed of light. Both $\boldsymbol{\alpha}$ and $\boldsymbol{p}$ are vectors

$$\boldsymbol{p} = (p_x, p_y, p_z) \equiv (p_1, p_2, p_3)\,,$$

$$\boldsymbol{\alpha} = (\alpha_x, \alpha_y, \alpha_z) \equiv (\alpha_1, \alpha_2, \alpha_3)\,.$$

To satisfy $E^2 = m_0^2 c^4 + p^2 c^2$ for (6.2), the following relationships must hold

$$\begin{aligned} \alpha_i \alpha_j + \alpha_j \alpha_i &= 2\delta_{ij} \\ \alpha_i \beta \; + \; \beta \alpha_i \; &= 0 \\ \beta^2 &= 1 \quad , \end{aligned} \tag{6.3}$$

where $i, j = \{1, 2, 3\}$ and the Kronecker delta, δ_{ij}, is defined using the Iverson bracket notation as $\delta_{ij} \equiv [i{=}j]$. Such a definition implies that all the components of $\boldsymbol{\alpha}$ and the $\boldsymbol{\beta}$ anticommute. They cannot be ordinary numbers. A possible representation satisfying the above anticommutation rules is a matrix representation. By defining an auxiliary vector $\boldsymbol{\sigma}$:

$$\boldsymbol{\sigma} = (\sigma_x, \sigma_y, \sigma_z) \equiv (\sigma_1, \sigma_2, \sigma_3) \tag{6.4}$$

constructed from the 2x2 Pauli matrixes

$$\boldsymbol{\sigma}_x = \begin{pmatrix} 0 & 1 \\ 1 & 0 \end{pmatrix} \qquad \boldsymbol{\sigma}_y = \begin{pmatrix} 0 & -\imath \\ \imath & 0 \end{pmatrix} \qquad \boldsymbol{\sigma}_z = \begin{pmatrix} 1 & 0 \\ 0 & -1 \end{pmatrix}, \tag{6.5}$$

the $\boldsymbol{\alpha}$ and $\boldsymbol{\beta}$ can be rewritten in a diagonal block-form

$$\boldsymbol{\alpha}_i = \begin{pmatrix} \mathbf{0} & \boldsymbol{\sigma}_i \\ \boldsymbol{\sigma}_i & \mathbf{0} \end{pmatrix} \quad \boldsymbol{\beta} = \begin{pmatrix} \boldsymbol{I} & \mathbf{0} \\ \mathbf{0} & -\boldsymbol{I} \end{pmatrix} \tag{6.6}$$

$$\text{where:} \quad \boldsymbol{I} = \begin{pmatrix} 1 & 0 \\ 0 & 1 \end{pmatrix} \quad \mathbf{0} = \begin{pmatrix} 0 & 0 \\ 0 & 0 \end{pmatrix}. \tag{6.7}$$

After applying the above relationships, the Dirac Hamiltonian, H_D, is (in cartesian coordinates)

$$H_D = \begin{pmatrix} p_0 - m_0c & 0 & -p_z & -(p_x + ip_y) \\ 0 & p_0 - m_0c & -(p_x + ip_y) & p_z \\ -p_z & -(p_x + ip_y) & p_0 + m_0c & 0 \\ -(p_x + ip_y) & p_z & 0 & p_0 + m_0c \end{pmatrix}, \tag{6.8}$$

with

$$p_0 = -\frac{\hbar}{ic}\frac{\partial}{\partial t}. \tag{6.9}$$

By inserting H_D into the equation (6.1), and based on the matrix multiplication rules, one concludes that the wave-function, Ψ_D, is a four-component vector.

An N-electron case

The Dirac equation (6.1) can be applied to N-electron problems. A central potential is considered first. In the first approximation, an instantaneous Coulomb potential may be introduced resulting in the N-electron Dirac-Coulomb equation

$$\left(\sum_{i=1}^{N} h_{D,i} + \sum_{i<j}^{N} \frac{1}{r_{ij}}\right) \Psi_D = E_D \Psi_D. \tag{6.10}$$

Despite its successes, the Dirac-Coulomb equation (6.10) exhibits certain fundamental problems. Introduction of the r^{-1} Coulomb potential is a serious approximation based on the non-relativistic assumption of instantaneous Coulomb interactions. In the relativistic framework, the distance r between a pair of interacting bodies in not the one that should be put into the potential. It reality, it should be a distance r' between the two interacting bodies at the moment the interaction reaches the other partner. The interaction process is fast, it occurs with the speed of light, but it is not instantaneous.

This lack of delay in the Coulomb potential results in a small, but experimentally measurable effect.

A partial remedy came from Breit. Breit introduced an additional term to the potential for pair-interactions

$$V_{ij}(r) = -\frac{1}{r_{ij}}\left[\frac{(\boldsymbol{\alpha}_i \cdot \mathbf{r}_{ij})\,(\boldsymbol{\alpha}_j \cdot \mathbf{r}_{ij})}{r_{ij}^2} + \boldsymbol{\alpha}_i \cdot \boldsymbol{\alpha}_j\right]. \tag{6.11}$$

Here the first term is the retardation term, it corrects for the interaction delay. The second term, known as the Gaunt correction, is a first, magnetic, correction to the Coulomb repulsion term. The Gaunt term has a particularly considerable effect on the inner-core region of the wave-function where the electrons move fast.

Putting Breit's correction (6.11) to (6.10) results in the N-electron Dirac-Coulomb-Breit equation

$$\left(\sum_i^N h_{D,i} + \sum_{i<j}^N \frac{1}{r_{ij}} - \sum_{i<j}^N V_{ij}(r)\right)\Psi = E\Psi. \tag{6.12}$$

Both the retardation- and Gaunt-corrections are comparable in size but opposite in sign. Thus, they should always be considered simultaneously.

6.2 The wave-function

The four-component Dirac wave-function Ψ_D

$$\Psi_D = \begin{pmatrix} \varphi_1 \\ \varphi_2 \\ \varphi_3 \\ \varphi_4 \end{pmatrix}, \tag{6.13}$$

can be formally rewritten as a two-component vector

$$\Psi_D = \begin{pmatrix} \phi_L \\ \phi_S \end{pmatrix}. \tag{6.14}$$

where

$$\phi_L = \begin{pmatrix} \varphi_1 \\ \varphi_2 \end{pmatrix}, \qquad \phi_S = \begin{pmatrix} \varphi_3 \\ \varphi_4 \end{pmatrix}. \tag{6.15}$$

The Hamiltonian (6.8) with external potential V, can also be written in the more compact 2x2 form

$$H_D = \begin{pmatrix} V + m_0c^2 & \boldsymbol{\sigma}\mathbf{p}c \\ \boldsymbol{\sigma}\mathbf{p}c & V - m_0c^2 \end{pmatrix}. \tag{6.16}$$

Using relations (6.15) and (6.16), the four-component Dirac equation simplifies to

$$\begin{pmatrix} V + m_0c^2 & \boldsymbol{\sigma}\mathbf{p}c \\ \boldsymbol{\sigma}\mathbf{p}c & V - m_0c^2 \end{pmatrix}\begin{pmatrix} \phi_L \\ \phi_S \end{pmatrix} = E\begin{pmatrix} \phi_L \\ \phi_S \end{pmatrix}, \tag{6.17}$$

where the ϕ_L and ϕ_S are the large and small components of Ψ_D, respectively.

By re-writing the Dirac equation (6.17) explicitly

$$\begin{aligned}(V + m_0c^2)\phi_L + \boldsymbol{\sigma p}c\phi_S &= E\phi_L \\ \boldsymbol{\sigma p}c\phi_L + (V - m_0c^2)\phi_S &= E\phi_S\end{aligned} \tag{6.18}$$

and using the second equation, the small component ϕ_S can be expressed in terms of the large component Ψ_L

$$\phi_S = \frac{\boldsymbol{\sigma p}c}{(E - V + m_0c^2)}\phi_L. \tag{6.19}$$

Eliminating the small component using relation (6.19), results in the two-component Dirac equation

$$(V + m_0c^2)\phi_L + \boldsymbol{\sigma p}c\frac{1}{(E - V + m_0c^2)}\boldsymbol{\sigma p}c\ \phi_L = E\phi_L, \tag{6.20}$$

Equation (6.20) is fully equivalent to the four-component counterpart.

6.3 Regular approximation

The two-component Hamiltonian (6.16), written in a more convenient metric, is

$$H_D = V + \frac{\boldsymbol{\sigma p}c\ K^{-1}\ \boldsymbol{\sigma p}c}{2m_0c^2 - V}. \tag{6.21}$$

Through the expansion of (6.21) in a power series with respect to K

$$K = \left(1 + \frac{E}{2m_0c^2 - V}\right), \tag{6.22}$$

the regular approximation is formulated. The expansion is formally an exact two-component representation of Dirac equation defined as infinite series. Already the zeroth-order term of the expansion introduces relativistic corrections to the non-relativistic limit. The Zeroth-Order Regular Approximation (ZORA) has the advantage of being variationally stable even for the heaviest known elements (up to Z=137). Higher-order approximations can also be defined (FORA - First-Order RA, $etc.$) although they are less-commonly used due to the small effect they introduce.

6.4 Perturbative corrections

The Dirac-Coulomb-Breit Hamiltonian (6.12) can be treated in a perturbative manner. It can be decomposed into the partial energy operators, H^i_{DCB}, with respect to the parameter $(\frac{Z}{c})^2$. Several important advantages are: the resulting operators H^i_{DCB} are computationally easy to implement and have well-defined physical interpretations.

The desired corrections can be added to the non-relativistic solutions in a very flexible manner. Within the first-order approximation:[38]

$$H^{I}_{DCB} = \sum_i \frac{\mathbf{p}_i^2}{2m_0} + V, \qquad V = -\sum_i \frac{Ze^2}{r_i} + \sum_i \sum_{i>j} \frac{e^2}{r_{ij}} \tag{6.23}$$

is the non-relativistic N-electron Hamiltonian.

$$H^{II}_{DCB} = -\frac{1}{8m_0^3c^2} \sum_i \mathbf{p}_i^4 \tag{6.24}$$

describes the mass-velocity dependence.

$$H^{III}_{DCB} = -\sum_j \sum_{i>j} \frac{e^2}{2m_0^2c^2} \left[\frac{\mathbf{p_i} \cdot \mathbf{p_j}}{r_{ij}} + \frac{(\mathbf{r_{ij}} \cdot \mathbf{p_i})(\mathbf{r_{ij}} \cdot \mathbf{p_j})}{r_{ij}^3} \right] \tag{6.25}$$

describes the 'orbit-orbit' interactions. It also partially accounts for retardation effects.

$$H^{IV}_{DCB} = \frac{e\hbar}{2m_0^2c^2} \sum_i \mathbf{s}_i \cdot \left[(-\nabla_i V) \times \mathbf{p}_i + \sum_j \sum_{j>i} \frac{2e}{r_{ij}^3} (\mathbf{r}_{ij} \times \mathbf{p}_j) \right] \tag{6.26}$$

is the 'spin-orbit' term. It describes the interaction between the orbital magnetic moments resulting from the orbital motion of charge, and the spin magnetic moments.

$$H^{V}_{DCB} = \frac{ie\hbar}{4m_0^2c^2} \sum_i [\mathbf{p}_i \cdot (-\nabla_i V)] \tag{6.27}$$

is the Darwin term. It does not have a classical characteristic.

$$H^{VI}_{DCB} = \frac{e^2\hbar^2}{m_0^2c^2} \sum_i \sum_{i>j} \left\{ -\frac{8\pi}{3} (\mathbf{s}_i \cdot \mathbf{s}_j) \delta^3(r_{ij}) + \frac{1}{r_{ij}^3} \left[\mathbf{s}_i \cdot \mathbf{s}_j - 3\frac{(\mathbf{s}_i \cdot \mathbf{r_{ij}})(\mathbf{s}_j \cdot \mathbf{r_{ij}})}{r_{ij}^2} \right] \right\} \tag{6.28}$$

is the 'spin-spin' interaction. The first term is the 'contact interaction', because it is non-zero only when the particles are at the same position. The second term is the interaction of the classical dipole-dipole type. Finally,

$$H^{VII}_{DCB} = \frac{e\hbar}{m_0c} \sum_i \left[\mathbf{H}(r_i) \cdot \mathbf{s}_i + \frac{e}{m_0c} \mathbf{A}(r_i) \cdot \mathbf{p}_i \right] \tag{6.29}$$

is the interaction between spin and orbital magnetic moments with an external magnetic field $\mathbf{H}(\mathbf{r_i})$.

6.5 Two-component methods

Attempt to solve the N-electron Dirac equation gives rise to solutions which are difficult to interpret. The existence of the continuum of negative energy eigenstates is counterintuitive for a chemist's concept of a ground-state bound system. Attempts have thus been made to make the relativistic equations simpler and more comprehensible.

6.5.1 Foldy-Wouthuysen transformation

The one-particle Dirac equation for a particle moving in the external field is

$$(c\boldsymbol{\alpha}\cdot\boldsymbol{\pi}+\boldsymbol{\beta}m_0c^2+eV)\Psi_D=E_D\Psi_D. \tag{6.30}$$

In general, any Hamiltonian can be represented as a sum of the 'odd' and 'even' operators, $\hat{o}$ and $\hat{\varepsilon}$:

$$\begin{aligned}\hat{\varepsilon}&=\tfrac{1}{2}(h_D+\boldsymbol{\beta}h_D\boldsymbol{\beta})\\ \hat{o}&=\tfrac{1}{2}(h_D-\boldsymbol{\beta}h_D\boldsymbol{\beta}).\end{aligned} \tag{6.31}$$

If the commutation rules

$$\begin{aligned}[\boldsymbol{\beta},\hat{o}]\ &=0\\ [\boldsymbol{\beta},\hat{\varepsilon}]_+&=0\end{aligned} \tag{6.32}$$

are satisfied, and

$$\hat{o}=c\boldsymbol{\alpha}\cdot\boldsymbol{\pi},\qquad \hat{\varepsilon}=e\Phi \tag{6.33}$$

then the 'odd' part of the Hamiltonian

$$(\hat{o}+\boldsymbol{\beta}mc^2+\hat{\varepsilon})\Psi_D=E_D\Psi_D \tag{6.34}$$

can be eliminated up to an arbitrary power of $(m_0c^2)^{-1}$.

Foldy and Wouthuysen applied a unitary transformation

$$UH_DU^{-1}U\Psi_D=UE_DU^{-1}U\Psi_D. \tag{6.35}$$

choosing the unitary operator U as

$$U=e^{iS}=\sum_{n=0}^{\infty}\frac{iS}{n!},\qquad U^{-1}=e^{-iS}=-\sum_{n=0}^{\infty}\frac{iS}{n!} \tag{6.36}$$

where $S=-i\beta\frac{\alpha p}{2m_0c}$. The third-order Hamiltonian becomes

$$\begin{aligned}H_D^{(3)}=&\left[\frac{\boldsymbol{\pi}^2}{2m}+m_0c^2-\phi\right]-\frac{e}{m_0}\boldsymbol{s}\cdot\boldsymbol{B}-\frac{\boldsymbol{p}^4}{8m_0^3c^2}\\ &+\frac{1}{8m_0^2c^2}(\boldsymbol{\nabla}\cdot\boldsymbol{E})-\frac{1}{2m_0^3c^2}S\cdot(\boldsymbol{E}\times\boldsymbol{p})-\frac{1}{2m_0^3c^2}(\boldsymbol{S}\cdot\boldsymbol{B})\,\pi^2.\end{aligned} \tag{6.37}$$

The resulting five-last terms can be used as first-order corrections to the non-relativistic result.

The Foldy-Wouthuysen (F-W) transformation reduces coupling between the electronic and positronic states. Unfortunately, decoupling of large and small components of Ψ_D affects also the operators. They are no longer variationally bound. Also, the F-W transformation can not be represented in closed form for a general potential, and can only be approximated. Despite the flaws, the F-W transformation provides solutions which fit more comfortably into traditional concepts of electronic solutions. It also is a good starting point for more advanced considerations.

6.5.2 Douglas-Kroll transformation

In 1974 Douglas, Kroll *et al.*[39,40] presented a method of decoupling the large and small components of Ψ_D. The Douglas-Kroll (DK) method starts with the first-order Foldy-Wouthuysen transformation, now performed in the momentum space. It is followed by a series of expansions in powers of the coupling strength parameter. The DK approach yields operators that are bound and can be conveniently used in the variational scheme.

The DK procedure starts from the unitary-transformation of the momentum-space defined Dirac Hamiltonian

$$UH_DU^{-1} = \hat{o} + \beta E_p + \hat{\varepsilon} = H'_D. \tag{6.38}$$

The transformation splits the Hamiltonian into the odd and even contributions now defined as

$$\begin{aligned} \hat{\varepsilon} &= A_p \left(V_x + R_p V_x R_p\right) A_p \\ \hat{o} &= \beta A_p \left[R_p, V_x\right] \end{aligned} \tag{6.39}$$

where:

$$A_p = \left(\tfrac{E_p+m}{2E_p}\right)^{\frac{1}{2}}, \qquad R_p = \tfrac{\boldsymbol{\alpha}\cdot\boldsymbol{p}}{E_p+m_0}, \qquad E_p = \left(\boldsymbol{p}^2 + m_0^2\right)^{\frac{1}{2}} . \tag{6.40}$$

Next, using the anti-hermitian operator W_1, a second unitary transformation, U'_1, is conducted

$$U'_1 = \left(1 + W_1^2\right)^{\frac{1}{2}} + W_1. \tag{6.41}$$

All coupling of the large and small component of the transformed wave-function are removed up to the first-order in V_x. As suggested by Douglas and Kroll, separation to arbitrary orders in the external potential is possible by a consecutive application of the operator

$$U'_n = \left(1 + W_n^2\right)^{\frac{1}{2}} + W_n. \tag{6.42}$$

up to the n-th order.

For most chemical purposes, truncating the decoupling at the second-order is sufficient. Higher-order contributions are typically important for the core electrons. Limiting the decoupling does not substantially affect the description of the valence space. The second-order Douglas-Kroll, one-particle Hamiltonian, H''_{DK}, is

$$H''_{DK} = E_p + \varepsilon_1 + \frac{1}{2}\left(\left[E_p, W_1^2\right]_+ + W_1 E_p W_1\right) \tag{6.43}$$

The Hamiltonian (6.43) may be employed in conjunction with the Coulomb potential to define an N-electron second-order Douglas-Kroll (DK2) Hamiltonian

$$H''_{DK} = \sum_{i=1}^{N} h''_{DK,i} + \frac{1}{2}\sum_{i,j}^{N} \frac{1}{r_{ij}} \tag{6.44}$$

A detailed investigations on heavy-atom-containing systems, proved the DK2 and higher-order DKn methods to be successful as compared to the fully relativistic results.[41,42]

6.5.3 Other Two-Component methods

The free-particle F-W transformation is performed in a basis representation. The DKH theory is nevertheless formulated as if it had been done at the operator level. Although formulation of the DKH transformation at operator level is possible, it makes it unnecessarily complicated, especially if higher orders are to be considered.

A first approximate quasi-relativistic theory, defined in a matrix form, was the so-called Normalized Elimination of the Small Component approximation of Dyall.[43] Filatov and Cremer[44] have cast the Regular Approximation into a matrix form, but the resulting equations were very lengthy even though they were only approximately correct.

In the context of the DKH approximation, the Infinite-Order Two-Component (IOTC) method of Barysz and Sadlej[45] emerged as the first $numerically\ exact$, quasi-relativistic two-component theory. The most impressive recent progress is of Kutzelnigg and Liu.[46] They proposed a scheme that contains as special cases a surprisingly compact version of Infinite-Order DKH as well as a very simple non-iterative method.

The idea of Kutzelnigg and Liu[46] was to start from the representation of the Dirac operator in a finite regular kinetically balanced basis. Then, a transformation is applied, that results in a quasi-relativistic Hamiltonian, expressed in the basis used for the upper component of the Dirac operator. The eigenstates of the new quasi-relativistic Hamiltonian are the same as those of the matrix representation of the Dirac Hamiltonian. Both the matrix and the operator formulation of the so-called Exact Two-Component (X2C) method are equivalent. According to the authors, the X2C Hamiltonian is currently the most robust and accurate among the available relativistic methods.

Chapter 7

Software

A number of software packages is currently available. Some program packages try to implement as many methods as possible, while other concentrate on a very specific range or even a single method. The results presented in this thesis were calculated using the following techniques and program packages:

MOLPRO: an extensive package of *ab-initio* programs for molecular electronic structure calculations. The emphasis is put on highly accurate computations, with extensive treatment of the electron correlation problem through multi reference CI, Coupled-Cluster and associated methods. Used here to calculate the Coupled-Cluster results.

TURBOMOLE: one of the fastest codes available for standard quantum chemical applications. Used here to calculate the HF/MP2 and DFT results, with and without the aid of RI approximations.

ADF: one of the few STO-based programs. ADF can treat all elements of the periodic table. ADF is especially suited for transition metal compounds. It contains state-of-the-art relativistic methods including ZORA and spin-orbit coupling to properly treat heavy nuclei at the all-electron level. It provides a wide range of approximate relativistic Hamiltonians allowing for relativistic vs non-relativistic comparisons. Used here for calculation of the spin-orbit effects.

Gaussian: designed for the needs of a user who does not necessarily possess an extensive theoretical background. With reasonable defaults for input data and the self-explanatory output it is probably the most intuitive and most widely used program package on the market. Used here for estimating anharmonic corrections to the vibrational frequencies.

VASP: An efficient and reliable package for performing *ab-initio* quantum-mechanical calculations using ultra-soft pseudopotentials and a plane-wave basis set. The interaction between ions and electrons is described using Vanderbilt pseudopotentials or the projector augmented wave method. Used as the main package for solid-state calculations.

Chapter 8

Results and Conclusions

8.1 New species

Quantum mechanics can be applied to calculate the properties of known molecules but it can also be successfully applied to inventing new species even before they are made.

8.1.1 Cyanides: MCN vs $M_3C_3N_3$ (M=Cu, Ag, Au)

The solid Group-11 cyanides MCN (M=Cu, Ag, Au) are well known. The experimentally determined structures correspond to hexagonally packed, infinite -M-CN-M-CN-chains[47] (see Fig. 8.1, A'). Following the study for Pyykkö *et al.*[48] on a possible new sheet structure of solid AuCN (see Fig. 8.1, B'), we predicted that the AgCN and CuCN could also have similar $M_3C_3N_3$ sheet structures. This new structure contains triazine-type six rings of three carbon and three nitrogen atoms, C_3N_3, which are coupled to each other by linearly coordinated metal atoms, forming a two-dimensional sheet structure. The sheets attract each other weakly due to the metallophilic attraction. For the

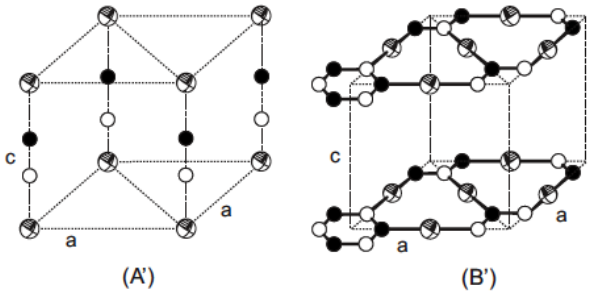

Figure 8.1: The (A') chain structure of MCN (P6mm), and the (B') sheet structure of $M_3C_3N_3$ (P$\bar{6}$2m). The spheres correspond to M, black circles to C and white circles to N atoms.

sheet structures, $M_3C_3N_3$ (M=Au-Cu), local energy minima were found for the simple stacking geometry with symmetry P$\bar{6}$2m (see Fig. 8.1, B'). The total energies for the chain and sheet structures at 0K are compared in Table 8.1. For CuCN and AgCN the energy differences are about 0.2 eV in favor of the chains. For AuCN there is practically no difference between the two structures, suggesting increased stability of the sheets.

Case	CuCN	AuCN	AuCN
3D sheet vs 3D chain	-0.22	-0.18	0.00
2D sheet vs 1D chain	-0.24	-0.21	0.03

Table 8.1: Total energy difference ΔE [eV] between the chain and sheet structures of Group-11 metal cyanides per MCN formula unit. A negative value indicates that the chain structure is energetically preferred.

8.1.2 Carbides: MC_2 vs M_3C_6 (M=Zn-Hg, Be-Ba)

Following the valence-isoelectronic principle, the transition metal dicarbides, MC_2 (M=Zn, Cd, Hg), and the alkaline-earth metal dicarbides, MC_2 (M=Be, Mg, Ca, Sr, Ba), were studied.

Excluding BeC_2, the remaining Group-2 dicarbides are experimentally known. Under normal conditions, MgC_2 adopts the tetragonal $P4_2/mmm$ symmetry, while the other carbides prefer the I4/mmm chain-like structure (see Fig. 8.2). For the known Group-2 dicarbides, the experimental structures were computationally reproduced and the calculated covalent bond lengths are in good agreement with experiment [Paper I].

On contrary, no reference data is available for the Group-12 dicarbides. For the MC_2 (M=Be, Zn-Hg), the three types of tetragonal packing presented in Fig. 8.2 were investigated. In all the cases tetragonal I4/mmm symmetry (Fig. 8.2, B) was preferred. No additional chain-like local-minima were identified.

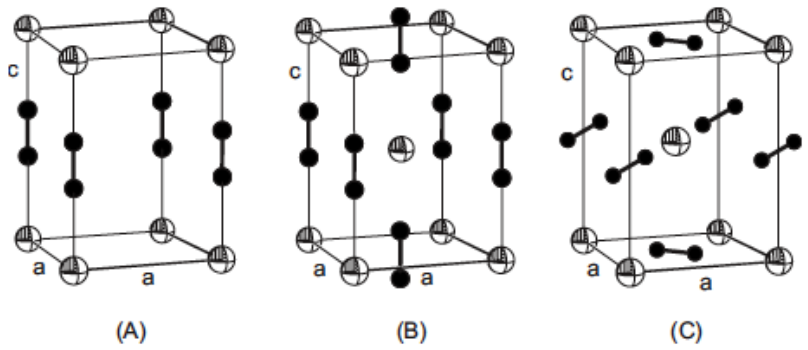

Figure 8.2: Investigated crystal structures for chain-type metal dicarbides MC_2 (M, spheres; C, black circles: (A) tetragonal P4/mmm, (B) tetragonal I4/mmm, and (C) tetragonal $P4_2/mmm$.

Isolated sheets: In the search of isolated, 2D M_3C_6 sheets, the previously identified hexagonal sheet-structure of cyanides was used as a starting point. Now, the six-member carbon rings are coupled together from the corners by the metal atoms (see Fig. 8.3, left). The calculations in this geometry, with a large sheet-sheet separation, yielded minimum energy structures for M=Be, Zn-Hg.

For the remaining metals, M=Ca-Ba, these 2D sheet spontaneously relaxed to a slightly different, hexagonal geometry. The carbon rings *rotated* by 30^o with respect to the initial structure (see Fig. 8.3, right). In this new structure, metal atoms are located

in the midpoint of the line connecting the C-C edges of every two benzene-like rings.

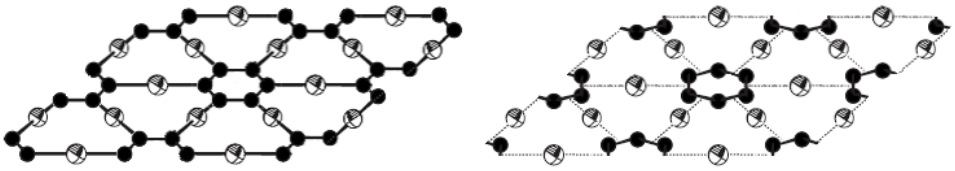

Figure 8.3: The two identified local sheet-like local minima for M_3C_6 carbides. The lest geometry was adopted by carbides with M=Be, Zn-Hg, while the right one by those with M=Ca-Ba.

Packed sheets: Considering 3D packing of the 2D sheet structures, a simple stacking analogous to cyanides was found purely repulsive for both *nonrotated* and *rotated* cases (D) and (F), respectively. Instead, an alternative 3D packing had to be introduced, with every second sheet translated by the vector v=($\frac{1}{2}$a, $\frac{1}{2}$a, 0) (see Fig. 8.4). For such systems, stable 3D geometries, (E) and (G), were found (Fig. 8.4).

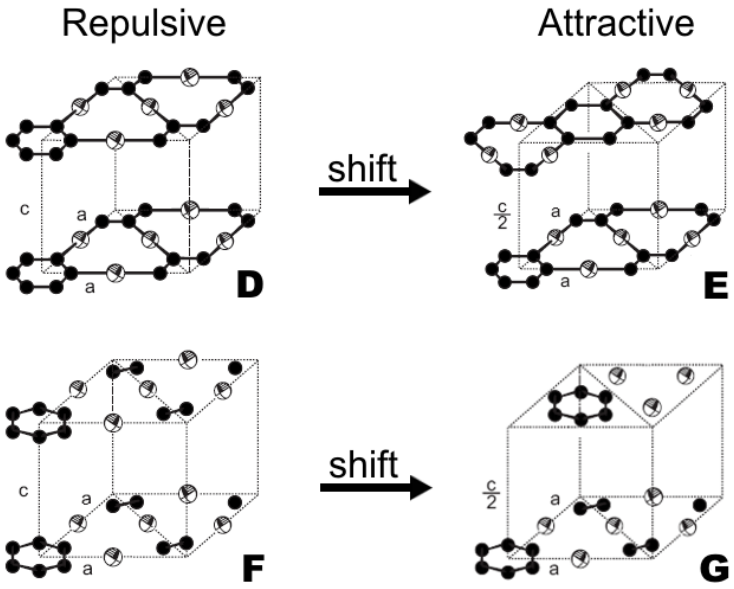

Figure 8.4: Investigated crystal structures for sheet-type metal dicarbides M_3C_6 (M=Be-Ba, Zn-Hg).

The structural preference with respect to the total energy is summarized in Fig. 8.5. The energy difference ΔE is given for each dicarbide per MC_2 unit. A negative value indicates that the chain structure is preferred. For the experimentally known dicarbides, M=Mg-Ba, the chains are energetically more stable, as expected. The energy difference roughly increases following Z, being in all the cases less than 1 eV. Interestingly, for the experimentally unknown dicarbides, M=Be, Zn, Cd, and Hg, the sheet structure is predicted to be more stable, and the energy difference likewise increases roughly following Z.

Electronic properties: Although DFT is known to underestimate band gaps, one can clearly see the general trends between the geometries and between the elements. In the case of both cyanide and dicarbide chain structures, all the known and predicted

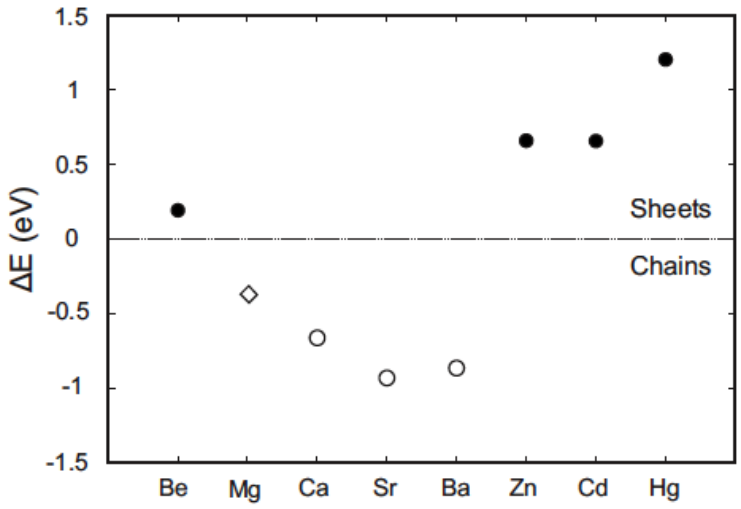

Figure 8.5: Total energy differences ΔE [eV] between the most stable chain and sheet structures for Group-2 and -12 metal dicarbides.

one-dimensional isolated and 3D structures are found to be insulators [Paper I]. For the packed dicarbide chain structures, the band gap is largest for the HgC_2 (3.7 eV) and smallest for BaC_2 (1.6 eV). The packed chain structures exhibit systematically smaller band gaps than the isolated chains due to the increased overlap of the valence orbitals. The only exception to this picture is BaC_2. All the predicted chain dicarbides, MC_2 (M=Zn-Hg), have larger gaps than the known dicarbides of Group-2.

For both the cyanide and dicarbide isolated 2D sheets, the band gaps are clearly smaller than for the chain structures. Furthermore, packing the sheets in a 3D structures decreases the band gap value even more.

For dicarbide sheets, we identify two candidates that appear metallic at the present DFT/GGA level of theory: Sr_3C_6 and Ba_3C_6. Both systems may have a significant amount of charge carriers. The rest of the cyanide and dicarbide compounds are found to be either insulators or semimetals with a slight band overlap between the occupied and unoccupied states.

8.1.3 Infinite, singly and multiply bonded chains and strips

A family of infinite 'nano-chains' and doubly-, triply- and multiply-bonded strips is predicted (Fig. 8.6). They consist of single, double or triple aromatic rings linked together by strong C-Au-C, C-Au←N or N→Au←N bonds. Depending on the system these 1D nano-structures are found to be insulators, narrow- or zero-gap semiconductors, or metals. Varying the nitrogen content in the aromatic rings is found to have a minor effect on the geometries.

The band structure of the 1D strips can be interpreted in a rigid-band picture. The orbital character of the states at the Fermi level has been analyzed indicating, in certain cases, similarities with the band structure properties of graphene.

A large number of $closed-shell$ species has been introduced and investigated (Fig.

8.6). Many of the systems contain a closed-shell C-Au←N bond, although stable systems can be found also for larger or smaller electron counts per bond. For instance, the present C-Au-C case is isoelectronic with the case where a coinage-metal cation bridges two N-heterocyclic carbenes with one extra conduction electron.[49]

Nano-chains: The simplest considered structures are the singly-bonded pyridine-based nano-chains (Fig. 8.6, **8a-8c**). The calculated polymerization energy of **8b** is 1.65 eV per monomer. As for the two other cases, **8a** and **8c**, it is 0.3 and 0.2 eV, respectively. Those systems will enjoy nearly free rotation of the monomers about the polymer axis. They would probably be much less stiff compared to the more complex strips. The calculated polymerization energy emphasizes the strength of the C-Au←N bond as compared to the C-Au-C and N→Au←N ones.

Double-ring nano-strips: The family of naphthalene-derived nano-strips **1a-1d** is depicted in Fig. 8.6. The calculated Au-Au distance are in the range of 255-270 pm, falling between the values in Au_2 dimer (247 pm) and bulk crystal (288 pm). The main feature in the final geometry of those strips is that the gold atoms protrude slightly from initial position due to the electrostatic repulsion, resulting in the C-Au←N angle being bent towards the strip edge.

Triple-ring nano-strips: Two types of anthracene-derived nano-strips are proposed. The first family is a straightforward analog of the double-ring structures, now with three bridging gold atoms (see Fig. 8.6, **2a-2e**). The middle bond is linear. The two lateral Au atoms are repelled by the central gold, leading to significant bending of the corresponding bonds.

The second family (structures **3a-3e**) is a modification of cases **2a-2e**. The central Au atom is now replaced by a hydrogen. The expected effect was to relieve the Au-Au repulsion. Indeed, as a consequence, the two lateral bonds return to linear positions.

For all the double- and triple-ring structures **1-3**, the C-N, Au-C and Au-N distances in the suggested new nano-strips are typical and similar with the distances calculated for $Au_3C_3N_3$ and M_3C_6 systems [Paper I]. For all the nano-strips discussed, the monomer geometries are found to be planar.

Ladder-type nano-strips In this proposal, two infinite poly-acenes are 'glued' by Au atoms. In the case of four structures, **4a-4d**, the Au-Au distance is to small hence the positively charged gold atoms strongly repel each other. Due to this unfavorable interaction, the structures are no longer planar. With alternating Au atoms being now 10-40 pm above and below the plane, the gold atoms form a zig-zag chain-structure. Nonetheless, even this kind of distortion does not prevent all four structures (**4a-4d**) from being unstable against vibrations. Only by replacing each second gold atom with hydrogen (see Fig. 8.6, **4e**) the steric tension is minimized and the resulting strip does not exhibit any imaginary frequencies.

Electronic properties: We found that a modification of the C/N content of the ring changes the orbital character of the Density of States (DOS) relatively little from a qualitative point of view. Therefore, as a first approximation, the DOS is interpreted

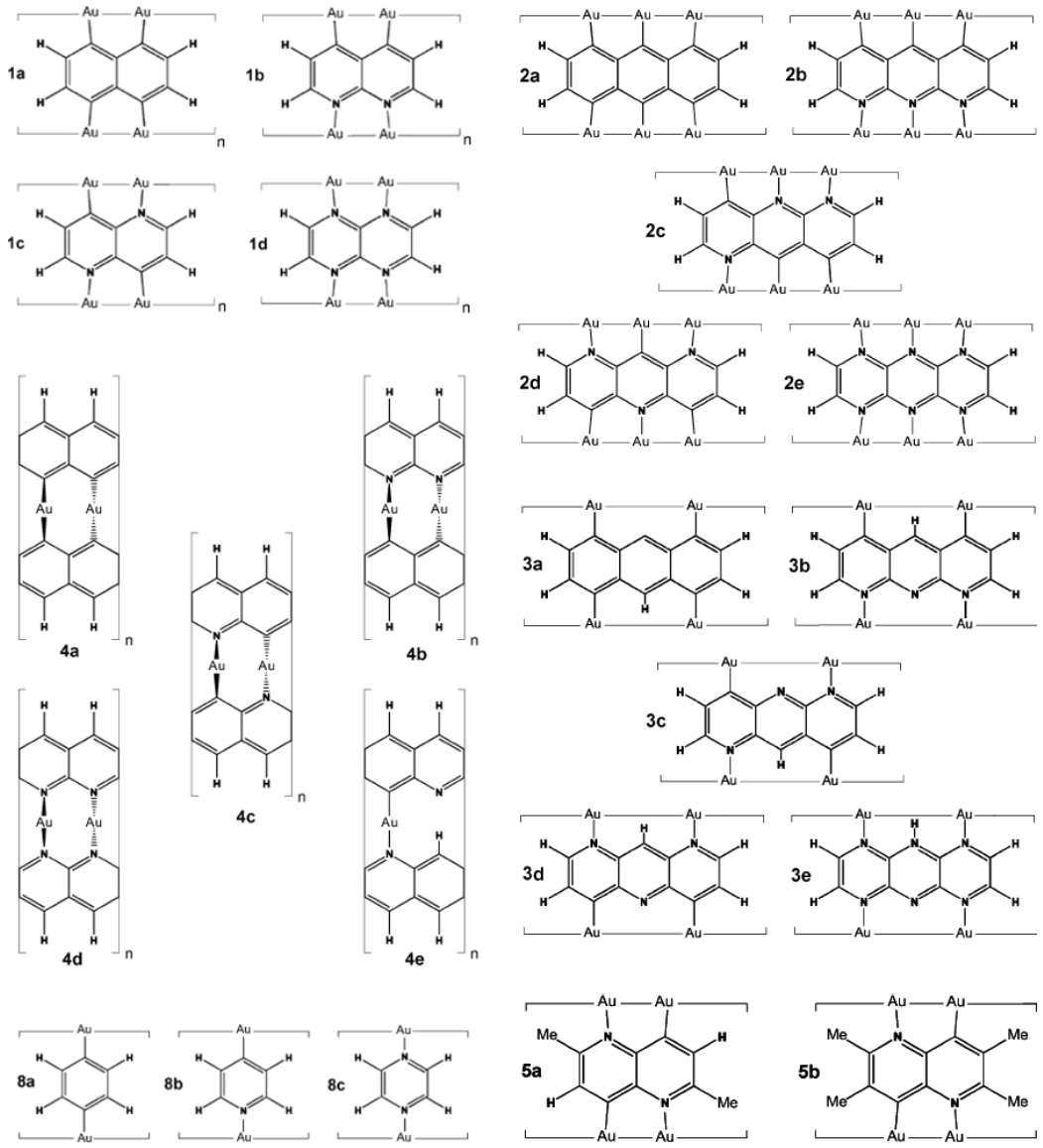

Figure 8.6: Series of proposed nano-chains and nano-strips.

in the rigid-band picture. In the C-rich cases, electrons are partially depleted from the saturated $2p_z$, $5d_{yz}$ and 6s orbitals, giving rise to a conduction band of a mixed character. Such systems could be thought of as having a 1D p-type band with contributions due to the metal valence $5d_{yz}$ and 6s electrons. In the N-rich cases, electrons are injected into the unoccupied $2p_z$ states, resulting in a p*-type conduction band. The addition of protective groups (Fig. 8.6, **5a, 5b**) was found to have very little effect on the band structure. The orbital character of the bands at E_f remained similar.

In general, the behavior of the double- and triple-ring cases **1** and **2** is similar, with one notable difference. The all-carbon structure **1a** is vibrationally unstable compared to the similar all-carbon **2a** case.

The ladder-type strips behave differently. Here, only the **4e** system was found stable against vibrations. In this system gold again acts only as a 'glue'. It was found that

the presence of the gold atoms does not strongly affect the electrical conductivity. The DOS shows that this system is a zero-bandgap semiconductor, and the states around the Fermi level have only p_z character, originating from the C and N atoms only. These states form a p-type valence and conduction bands. Those valence bands which have Au orbital character are particularly flat, suggesting negligible Au orbital interaction along the strip. Intriguingly, the conduction band of graphene is also formed from the $2p_z$ orbitals and has zero-bandgap semiconductor properties. In graphene the p-band has no overlap with the filled valence bands (2s, $2p_x$, $2p_y$), whereas in proposed **4e** the p-band crosses the d-bands as one moves off the Γ-point.

8.1.4 Finite, gold-glued nano-strips and nano-rings

Gold atoms can act as an 'intermolecular glue', coupling (hetero)aromatic rings, typically through C-Au←N bonds. An example on gold-glued poly(triaurotriazine) sheets, and infinite nano-strips was already discussed. Although the sheets [Paper I] and the infinite nano-strips [Paper II] are yet experimentally unknown, the chemically stable dimers and oligomers of 2,6-diauro-1,5-naphthyridine molecule are known.[50,51] We investigated several such finite nano-strips. We also propose to bend the strips to form 'gold-glued' naphthyridine-based cylindrical structures with n monomeric units (n=4-10).

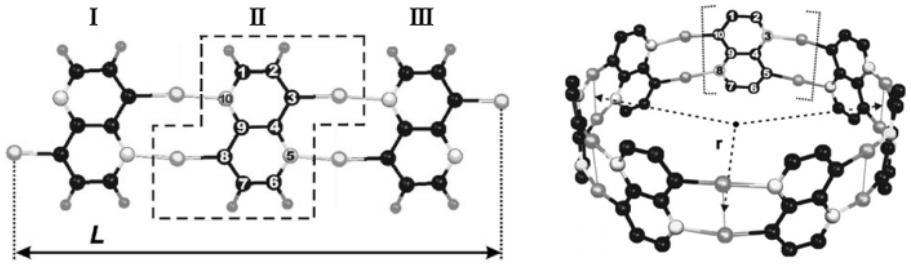

Figure 8.7: The notation scheme for strips and rings.

Nano-strips: The simplest member of the strip family is the 2,6-diauro-1,5-naphthyridine molecule. Both the molecule, and the longer strips were optimized with C_{2h} symmetry (Fig. 8.7, left). The geometry optimization did not reveal any significant bond length alternation for longer strips. The vibrational analysis shows only real frequencies. Selected results are given in Table 8.3.

Length \ n	4	5	6	7	8	9	10
N_3-Au	214.6	213.5	213.3	213.0	212.9	212.8	212.7
C_5-Au	200.6	200.4	200.4	200.4	200.4	200.4	200.4
Au-Au	274.4	272.8	272.4	271.7	271.4	271.2	271.1
r	442.4	553.4	6.411	775.9	871.1	998.5	-

Table 8.2: Calculated bond lengths and radius, r, for polynaphthyridine rings. For the atom notation, see Fig. 8.7. All values in pm.

	$n=1$	$n=2$		$n=3$			$n=4$			
Length	I	I	II	I	II	III	I	II	III	IV
C_3-Au	197.9	200.7	197.7	200.6	200.5	197.7	200.6	200.4	200.5	197.7
C_8-Au	197.9	197.7	200.7	197.7	200.5	200.6	197.7	200.5	200.4	200.6
N_5-Au	-	212.8	-	212.7	212.8	-	212.7	212.6	212.8	-
N_{10}-Au	-	-	212.8	-	212.8	212.7	-	212.8	212.6	212.7

n	1	2	3	4	5	6	7	8	9	10
L	678.7	1376.6	1675.0	2772.9	3870.8	4968.7	6066.6	7164.5	8262.4	9360.3

Table 8.3: Selected bond lengths and strip lengths, L, tabulated for selected flat polynaphthyridine systems (for the monomer notation and bond description, see Fig. 8.7).

Nano-rings: Six naphthyridine-based rings with the number of $Au_2C_8N_2H_4$ monomeric units varying from 4 to 10 are predicted and investigated. All systems were relaxed with fixed D_n symmetry (Fig. 8.7, right). Each ring can be viewed as n (hetero)aromatic monomers 'glued' together by gold atoms. We did not observe any significant alternation between the rings with odd and even n. Interestingly, the N-Au and the Au-Au bond lengths decrease slightly for larger systems, while the Au-C distances remain practically the same. The qualitative bonding analysis indicates that the present (hetero)aromatic monomers appear to be simply 'glued' together by gold atoms. The predicted rings could also exhibit interesting dispersion interactions with atoms or molecules inside them.

Mechanical properties: We found all the considered strip and ring structures stable with respect to vibrations. To get additional feeling for the mechanical rigidity of proposed rings we bent the finite nano-strips to rings and compared that bending energy with the one for polyacene rings with similar dimensions. Apart from the energy needed to create the ring from a linear strip, we also used the in-plane deformation vibrational frequencies as a criterion for rigidity. The analysis is described in more detail in Section 8.2.

8.1.5 Aurocarbons

Gold is noble, but its chemistry is fascinatingly rich. One of the interesting aspects of gold chemistry is the analogy between Au and H. Recently Naumkin[52] considered the possibility of completely 'aurating' neopentane, $C(CH_3)_4$. Concerning the gas-phase, the dication CAu_2^{2+} was mass-spectroscopically observed by Gibson.[53] Its electronic structure was interpreted by Pyykkö *et al.*[54] as $[Au{=}C{=}Au]^{2+}$, with bonding similar to that of O=C=O. Pyykkö *et al.* also considered the D_{3h} cation CAu_3^+, also observed by Gibson, and the yet unknown neutral C_2Au_2 that could be directly compared to C_2H_2. For other examples on gold-acetylide bonds, see the works of Puddephatt *et al.*. Furthermore, a solid C_2Au_2 has been reported to be highly explosive.[55]

The chemical analogy of Au and H is an important conceptual tool in predicting new possible species. Based on it, the series of simple neutral aurocarbons (Fig. 8.8): CAu_4, C_2Au_2, C_2Au_4, C_2Au_6, and C_6Au_6 were investigated using DFT and the MP2 theory.

The vibrational frequencies and the bonding mechanism were investigated.

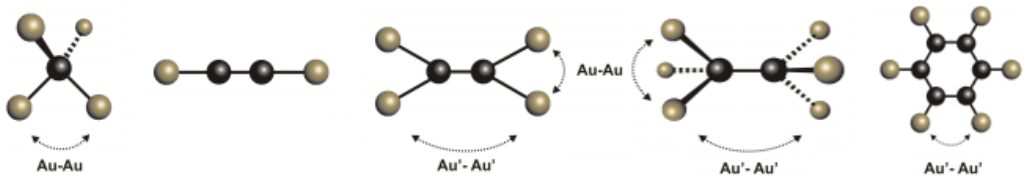

Figure 8.8: The series of simple, uncongested aurocarbons.

Geometries: The schematic equilibrium structures are depicted in Fig. 8.8. Both the TPSS and B3LYP results agree well with each other. The average difference for those two functionals is 0.93 pm for the C-C bond, and the difference in the Au-C bond length is 2.15 pm.

The MP2 and DFT structures differ slightly. One clear trend is that the MP2 metal-metal distances are always the shortest, as compared to the DFT results. This is expected due to the MP2 known exaggeration of bonding for such organometallic bonds.

The Au-C distance varies from one molecule to the other by up to 12 pm. It depends strongly on the type of the C-C bond. It shortens with the hybridization as $sp < sp^2 < sp^3$. The Au'-Au' (see Fig. 8.8) distances show only weak aurophilic interactions, while the Au-Au distances are expected to have much stronger ones. The C-C distances in the C_2Au_2, C_2Au_4 and C_2Au_6 are closely comparable with the corresponding hydrocarbons suggesting analogous bonding.

Bonding: The calculated Kohn-Sham orbitals (TPSS) correspond to the combinations, expected from the existing C-C and Au-C local bonding orbitals [Paper VI]. An example on C_2Au_6 is depicted in Fig. 8.9. The simplest way to understand the frontier bonding orbitals of C_2Au_6 is to classify the bonding orbitals HOMO to HOMO-4, and HOMO-9, as the e_g ($\times 2$), t_{1u} ($\times 3$), and a_{1g} combinations of the six Au-C local bonding orbitals under octahedral, quasi-O_h symmetry. The corresponding nodal structures are then conspicuous in Fig. 8.9.

Thermodynamical stability: The thermochemical analysis for a series of reactions was performed with respect to several starting reagents.

The analysis performed with respect to the isolated Au_2 and the $C(^3P_J)$ atoms yields the strongly negative formation energy of the CAu_4 and C_2Au_2 for all applied methods. The energy of Au_2 addition to the C_2Au_2 and C_2Au_4 remains negative for TPSS and MP2 but changes sign in case of B3LYP results. The trimerization energy of C_2Au_2 is strongly exothermic.

To make sure that the broken chemical bonds are of the same type as the type of bonds formed in the reaction, we applied the isodesmic approach. The DFT formation energy calculated per one Au-C bond is approximately constant for a given functional. Interestingly, the same energy calculated at MP2 level decreases systematically in the C_2Au_n (n=2, 4, 6) series and becomes thermo-neutral for C_2Au_6, most likely due to

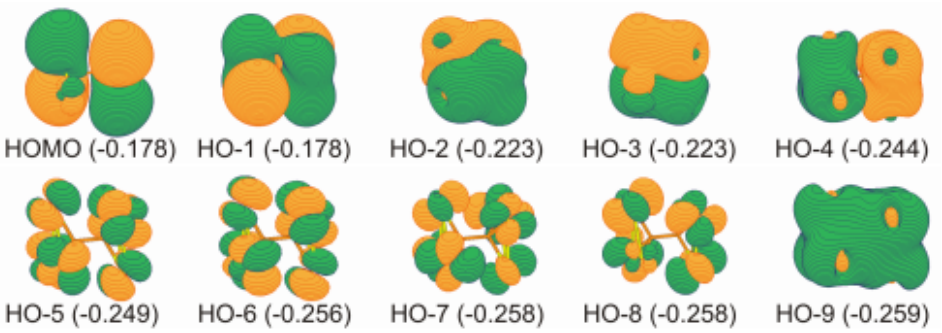

Figure 8.9: Selected occupied Kohn-Sham (TPSS) molecular orbitals of C_2Au_6 (D3d). The LUMO orbital energy is -0.130 a.u., resulting in a HOMO-LUMO gap 1.31 eV (HO-n stands for HOMO-n).

aurophilic stabilization.

8.1.6 Au_nHg_m clusters

The structures of metal clusters are of current interest. A large number of alternative structures is already known, both for neutral and charged gold-containing clusters. For a review on the current progress in gold-cluster chemistry see Refs.[1,2]

Perhaps surprisingly, the neutral Au_nHg_m clusters, particularly with more than one Hg atom, have not been previously studied. Rykova *et al.*[56] treated Au_nM (M=Hg, E112). The simplest diatomic gold/mercury species, $AuHg^+$, was considered by Wesendrup *et al.*[57]

We first asked the question whether the diaurides, Au-M_m-Au (m=1, 2), or the 'digold amalgam molecules', Au-Au-M_m, would be preferred. A further question is that of planarity versus nonplanarity for these metal clusters. Selected possible structures of the present species are shown in Fig. 8.10.

We also note that the closed-shell pure mercury chain cations Hg_2^{2+}, Hg_3^{2+}, and Hg_4^{2+} are known in solids.[58,59,60,61] We thus propose the possible mixed isoelectronic species $[HgAuHg]^+$. A similar 'inverted' case, a triatomic two-valence-electron $[AuHgAu]^{2+}$, was synthesized in a solid by Catalano *et al.*[62]

Geometries: In all the three-, four- and five-atom cases, a number of local minima were identified. Selected results for larger clusters are given in Fig. 8.10. For the larger clusters, the primary question was that of planar vs nonplanar nature. We performed an extensive search for nonplanar isomers but found only strictly planar ones.

Au_2M (M=Zn-Hg): In general, for triatomic A_2B species, three types of arrangement are possible: two linear and one triangular. We found that linear conformations were always preferred. The relative energies of the Au-Au-M and Au-M-Au linear arrangements actually depend on M. For zinc and cadmium, structures with terminal gold atoms are preferred, while mercury prefers to bind to the end of an Au_2 unit. These cases could be called Zn and Cd diaurides and a molecular gold amalgam, respectively.

Going from zinc to cadmium, the Au-M distance increases significantly by ~20 pm, whereas going from cadmium to mercury there is practically no increase in the bond

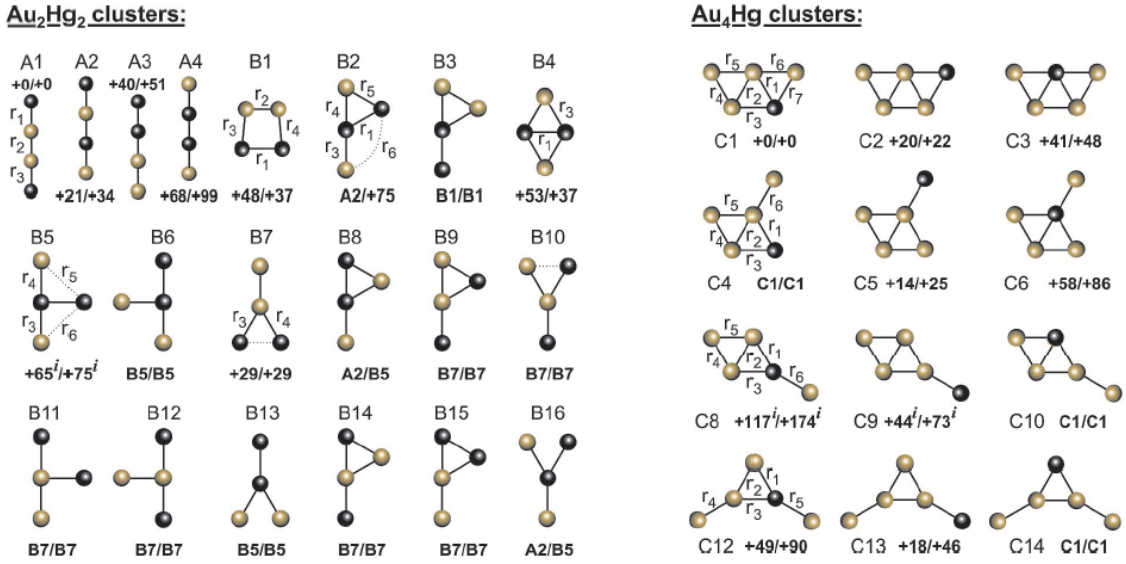

Figure 8.10: Schematic representation of *selected* investigated structures. The relative energy [kJ mol^{-1}] with respect to the energetically lowest structure is given for the meta-stable structures. The two energies are given at DFT/MP2 levels, respectively (i indicates a transition state.)

length. This is yet another example of the relativistic bond-length contraction.

Au_2Hg_2: Among the linear structures, four local minima were identified. The total energy comparison indicates that the **A1**, 'gold amalgam' (Hg-Au-Au-Hg), is preferred and the **A4**, a linear mercurous diauride (Au-Hg-Hg-Au), lies highest. The direct structural comparison of **A1** (Hg-Au-Au-Hg) with the triatomic Au-Au-Hg reveals similarities in bonding. Both lower symmetry cases, **A2** and **A3**, have intermediate energies. In the case of **A2** (Hg-Au-Hg-Au), one can distinguish a tightly bound Au-Hg-Au 'core' and a mercury atom more weakly bound to it. The **A3** is particularly interesting due to the very long Hg-Hg distance, r≈300 pm. The **A3** structure could be considered as a rather weak Hg· · ·Hg-Au-Au vdW complex.

During the geometry scan, several planar local minima were identified, with Y-shaped **B7** being the most stable. Among other, the **B7** structure is remarkable in having an essentially undeformed Au_2 unit with two Hg atoms coordinated to it at a large distance from each other. It may deserve further study at more sophisticated levels. Several transition states are possible and a large number of local minima were identified, all of them planar.

Au_4Hg: For the five-atomics, the **C1** structure, in which a mercury atom is bound to three adjacent gold atoms, emerged as the energetically most preferable. It is qualitatively similar to the structure of the isoelectronic[63] Au_5^-. Many structurally similar structures, such as 'half-cake' structures **C2** and **C3**, do not lie much higher. Varying the coordination site gives many isomers that are close in energy (see Fig. 8.10).

Charged species: In addition to neutral three-atom species, the cationic, two-

valence-electron $[AuHgAu]^{2+}$ was also calculated. It is experimentally known in the solid state.[62] The experimental structure is linear with $r_{\mathrm{Au-Hg}}$=278 pm. Our free-ion DFT calculation actually prefers a C_{2v} triangular structure (with $r_{\mathrm{Au-Hg}}$=269 pm) by approximately +58 and +78 kJ mol^{-1} at DFT and RIMP2 levels, respectively.

Four-atom charged species were also investigated. The isoelectronic Au_4^{2-} is proposed as a possible anion in alkali aurides, alkali solutions in liquid ammonia, or similar reducing surroundings. Some occupied MOs of the free ion will then have positive energies, corresponding to continuum states. Concerning Au_4^{2-} at the DFT level, a linear isomer was found to be energetically lowest, with the D_{3h} 'star' ($r_{\mathrm{Au-Au}}$=266.88 pm), and the D_{4h} square ($r_{\mathrm{Au-Au}}$=269.07 pm) higher by +80 and +130 kJ mol^{-1}, respectively. At the MP2 level, a linear isomer was still favored, now followed by a C_{2v} rhombus and the D_{3h} star higher. In the case of the isoelectronic Hg_4^{2+} ion, a linear isomer was found to be energetically preferred at both the DFT and MP2 levels. The D_{3h} isomer lies higher by +100 kJ mol^{-1} and the D_{4h} square by +65 kJ mol^{-1}.

Concerning the structures, both the Hg_4^{2+} and the isoelectronic Au_4^{2-} chains have shorter bonds at the ends compared with those at the middle in both our free-molecule calculations and the solid-state experiment.

Most of the proposed species are new. The likely ways of making these species may involve highly nonequilibrium conditions. Several possible formation paths were discussed in more detail in Paper VII.

8.2 Molecules as elastic bodies

The flat 2,6-diauro-1,5-naphthyridine polymers, discussed in Section 8.1.3 were bent to closed rings with up to 12 monomers. The structural properties of the rings and the corresponding flat strips are discussed in Sections 8.1.3 and 8.1.4. In this section we focus on their vibrational properties, particularly bending energies and lowest in-plane deformation frequencies.

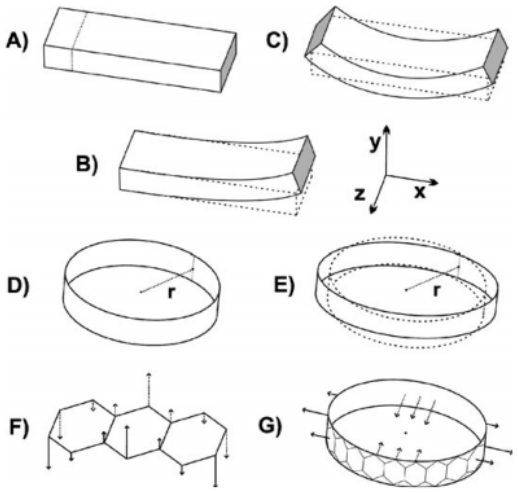

Figure 8.11: Schematic illustration for the bar-type and the ring-type systems. Examples on the considered vibration modes are depicted in F and G.

To understand the connection between the elastic deformation energies, and the vibrational frequencies of the finite strips and rings, we first looked at their classical counterparts. Consider first a bar segment, as in Fig. 8.11, B. The potential energy contribution due to bending is[64]

$$dV = \frac{EI}{2}\left(\frac{\partial^2 y}{\partial x^2}\right)^2 dx, \tag{8.1}$$

where E [N m^{-2}] is the Young modulus and I [m^4] is the cross-section inertial. The equation (8.1) corresponds to properties of macroscopic objects and cannot be applied for single molecules.

Let us then consider a ring of radius r. For such a system

$$\frac{\partial^2 y}{\partial x^2} = \frac{1}{r}, \tag{8.2}$$

hence the total bending energy of the ring,

$$V = \pi\frac{EI}{r}. \tag{8.3}$$

Following den Hartog,[64] the lowest vibrational angular frequency of a 'free-free bar' (Fig. 8.11, C) is

$$\omega = \frac{\pi^2}{2\sqrt{\frac{1}{4} - \frac{2}{\pi^2}}} \sqrt{\frac{EI}{\mu L^4}} \tag{8.4}$$

where L is the length, m the mass and μ = m/L the mass per unit length of the bar. Note that ω behaves as L^{-2}. For arbitrary vibrational mode of a ring of radius r in its own plane, the results of Hoppe[65] and Love,[66] together with (8.3) give

$$\omega = \frac{n(n^2-1)}{r^2\sqrt{1+n^2}} \sqrt{\frac{rV}{\pi\mu}} \tag{8.5}$$

where n is the number of wavelengths along the ring. This yields a consistency check between V and ω

$$\frac{\omega^2}{V} = \frac{1}{r^3\pi\mu} \frac{[n(n^2-1)]^2}{1+n^2}, \tag{8.6}$$

which for the lowest mode of the in-plane ring vibration (n=2) gives

$$\frac{\omega^2}{V} = \frac{72}{5} \frac{1}{r^2 m} = 14.4 r^{-2} m, \tag{8.7}$$

with m being now the total mass of the ring molecule. By comparing (8.4) and (8.5) and setting n=2, one finds that the ring of radius r has the same lowest frequency as a bar of length L so that

$$\frac{L^2}{r^2} = \frac{\pi^3}{6} \sqrt{\frac{5}{\pi^2 - 8}} = 8.45, \tag{8.8}$$

which in turn corresponds to L/r = 2.90, approximately half the ring perimeter.

The low-lying vibrational frequencies should thus behave as L^{-2} and r^{-2} for the strips and rings, respectively. The energy of bending a flat system to a ring of radius r should go as r^{-1}. We now apply these laws to quantum chemical results.

The analysis of the lowest vibrational modes: Vibrational frequencies were calculated for the considered strip- and ring-type molecules within harmonic approximation. We focus on the energetically lowest-lying modes, corresponding to the macroscopic vibrational modes of the stiff slab and the ring (see Fig. 8.11).

Our results calculated for n=2 confirm the $\omega(L^{-2})$ and $\omega(r^{-2})$* behavior predicted by (8.5). The selected results are presented in Fig. 8.12. For the two higher vibrational modes, corresponding to the n=3 and n=4, we also observed similar trends. The calculated ratios of slope coefficients for polyacenes: 1:2.32:4.21, are comparable to the theoretical values of 1:2.82:5.42 obtained from (8.6) [Paper III, Fig. 9].

For higher values of n, the shortest polyacene 'bars' had to be excluded from consideration. With larger n they were found to be too 'short' to reproduce the higher-order

*Note that L=$2\pi r$

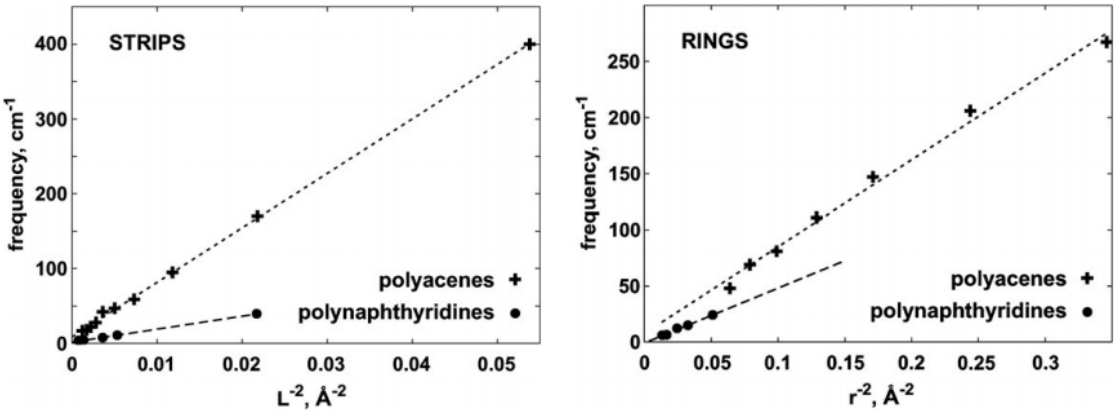

Figure 8.12: The $\omega(L^{-2})$ dependence for finite strips (left) and $\omega(r^{-2})$ dependence for rings (right) calculated for corresponding polyacene and polynaphthyridine molecules. For the description of considered deformations see Fig. 8.11, F and G.

vibrations with larger number of nodes. Similar trends were observed for naphthyridine series.

The considered vibrational frequencies indeed behave as predicted by the classical model, i.e. they are proportional to the length parameter r or L to the power -2. A similar approach using the Hoppe solution was used by Ceulemans and Vos to discuss the ring vibrations of benzene.[67] The approach was also extended to spheres, modeling icosahedral fullerenes.[67,68]

To our best knowledge, we report the first observation, that a molecular *sequence* behaves in this respect as a series of elastic bodies.

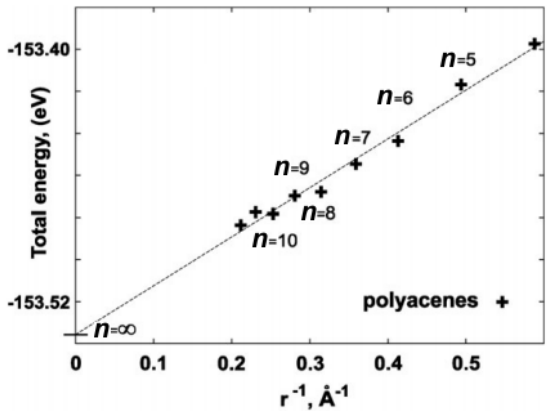

Figure 8.13: An example on the extrapolation scheme applied to the polyacene rings. The $n{=}\infty$ corresponds to the energy value on one $[C_2H_4]$ unit in the ring of infinite diameter.

The energies of bending strips to rings: The difference of the $[C_2H_4]$ block between the corresponding polyacene rings and strips, makes the direct comparison impossible. On contrary, the naphthyridine rings are just bent strips, with the same general formula, $[Au_2C_8N_2H_4]_n$, although an extra complexation energy still arises.

Because the closing energy of an infinite polyacene ring is unknown, it impairs simple attempt to determine the energy required for bending a strip into a ring, through their total energies. Therefore an alternative reference for the energy of a flat, infinite polymer was obtained by letting the ring radius approach infinity, see Fig. 8.13. We define the extrapolated energy value, $E_{Ring}(\infty)$, as the energy of one [C_2H_4] block in the ring of infinite diameter. The energy of bending an n-block strip into the ring can then be defined as:

$$\Delta E_{Ring}(n) = E_{Ring}(n) - E_{Ring}(\infty). \tag{8.9}$$

Here the $E_{Ring}(n)$ is the total energy of *one* [C_2H_4] unit in the n-unit ring, and the $\Delta E_{Ring}(n)$ is the excess energy per one monomer unit. The total bending energy, V, of equation (8.3) can then be calculated as

$$V = n \cdot \Delta E_{Ring}(n).$$

Already from Fig. 8.14 one notices that the bending energy indeed behaves as r^{-1}, just as expected from (8.9).

Based on (8.7) we also performed a consistency check between the bending energies obtained from (8.9) and the lowest frequency modes (n=2). The results are depicted in Fig. 8.14. The fitted slopes of the two lines were calculated to 14.32 and 13.64 for the polyacene and polynaphthyridine systems, respectively. These can be compared to the theoretical slope of 72/5=14.4, predicted by equation (8.7).

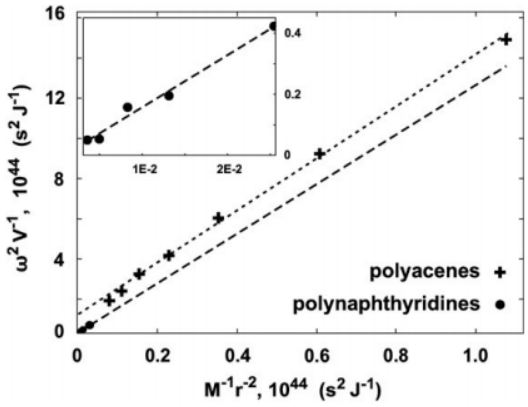

Figure 8.14: A consistency check between the calculated vibrational frequencies and bending energies. The slopes of the two fitted lines were calculated to 14.32 and 13.64 respectively, as compared to the theoretical slope of 14.4 calculated from (8.7).

8.3 Basis-set limit of the aurophilic interactions at MP2 level

Many experiments[69,70] suggests that, at equilibrium distances of the order of 300 pm, two Au(I) cations in compounds may experience an *attraction* of the order of 30-40 kJ mol^{-1}. This phenomenon, known as the aurophilic attraction,[71] has been extensively studied both experimentally and theoretically. For reviews see Ref.[1,72]

The earliest molecular study (1985) on closed-shell Au(I)-Au(I) systems was of Hoffmann *et al.*[73] He attributed the aurophilic attraction to the effect of hybridizing the 6s, 6p, and 5d orbitals of gold. In 1991 Pyykkö and Zhao ascribed this attraction to the electron correlation effect.[74] Later in 1997, Pyykkö and Mendizabal provided first conclusive evidence for the dispersive nature of the attraction.[75,76] They pointed, that at large distances its strength decreases as R^{-6}. Later studies indicate that close to the equilibrium Au(I)-Au(I) distance, contributions from virtual charge-transfer terms may also be important.[77]

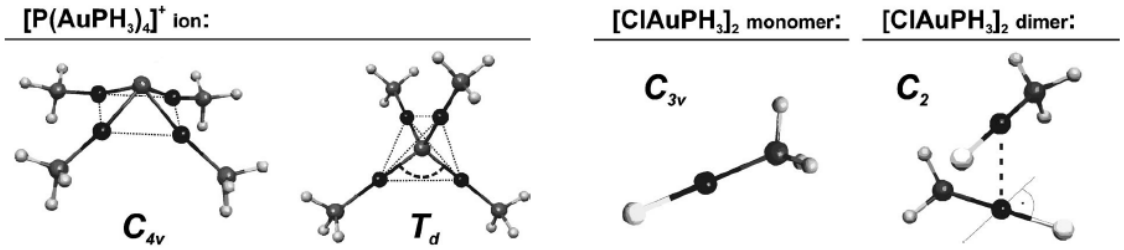

Figure 8.15: The C_{4v} and T_d structures of the $[P(AuPH_3)_4]^+$ ion, C_{3v} structure of the $ClAuPH_3$ monomer and C_2 structure of the perpendicular $[ClAuPH_3]_2$ dimer.

The applied methodology evolved with time but the studied model remains the same. The commonly accepted system for studies on aurophilicity is the perpendicular dimer $[ClAuPH_3]_2$ (Fig. 8.15). Its dimerization energy corresponds to the aurophilic attraction. As suggested by Li and Pyykkö already in 1992,[78] due to the nature of this weak intermolecular interaction, the basis-set superposition error (BSSE) corrections must be introduced. For accurate reproduction of aurophilic attraction certain basis functions must also be present in the gold basis set. The diffuse s-, p- and d-type functions were found to have little effect. On the contrary, the f-functions were found to be particularly important. In 1992 Li and Pyykkö introduced a diffuse f-function ($\alpha = 0.20$) that maximizes the Au^+ static polarizability, and a tight polarization f-function with $\alpha = 1.19$. Higher angular-momentum functions have been included for gold by Magnko et al.[79] The basis size of ligands has been studied,[80] and was found particularly sensitive for soft atoms. The *basis-set limit* of the aurophilic interaction has not been earlier critically investigated. We now investigate it at the MP2 level. We also compare two 19-VE pseudopotentials of Andrae *et al.*[81] and the recent one of Figgen *et al.*[82]

An additional motivation for such a study is the conflicting results for the preferred conformations of the tetra-aurophosphonium cation (Fig. 8.15), $P[AuPH_3]_4^+$, in Ref.[80] versus Ref.[83] Following the experimental observation of Zeller *et al.*,[84] that the $[As(AuPPh_3)_4]^+$ ion in solid $[As(AuPPh_3)_4]^+[BF_4]^-$ is pyramidal (C_{4v}) and not tetrahedral (T_d), Li and Pyykö verified the result using *ab-initio* calculations. In their calculations the $[N(AuPH_3)_4]^+$, the T_d symmetry was preferred, also in agreement with

the experiment. For $[P(AuPH_3)_4]^+$, a clear preference for C_{4v} was obtained (-90.3 kJ mol^{-1}). The latter result was supported by Pyykkö and Tamm[85] (-76.5 kJ mol^{-1}) but it was recently contested by Fang and Wang[83] (+84 kJ mol^{-1}).

$[ClAuPH_3]_2$ dimer: The effect of choosing the Andrae or Figgen 19-VE pseudopotential on the interaction energy ΔE and the Au-Au distance, R, was found to be small. The difference in ΔE, due to the choice of PP, reaches up to 0.15 kJ mol^{-1}. The difference in R_e increases slightly with basis size but remains less than 0.5 pm even for the largest considered basis. Different pseudopotentials yield a negligible error [Paper IV, Table 2].

For the study on the basis-set limit, several Karlsruhe split-valence basis sets (def-X and def2-X, X=SVP-QZVPP) and their augmented versions were applied. The augmentation refers to adding two f-type functions (α=0.20, 1.19) of Pyykkö et al.[80] All considered basis sets were augmented using two schemes: the f-functions were added as uncontracted (-A), and contracted (-B). Application of bases with two uncontracted f-functions for Au, lowers the value of ΔE_{CP} and leads to faster and more systematic convergence.

The previously reported ΔE_{CP} for dimer, calculated by Li and Pyykkö[80] was obtained with approximately TZVP-quality basis set with two $uncontracted$ f-functions and with Andrae ECP applied. The resulting value of -24.70 kJ mol^{-1} corresponds to the presently reported value of -22.94 kJ mol^{-1} obtained with a slightly larger Karlsruhe def2-TZVP basis set augmented with the two f-functions for consistency.

The basis-set size dependence of the counterpoise correction to the calculated ΔE was investigated. The differences between counterpoise-corrected ΔE_{CP} and uncorrected ΔE values are depicted in Fig. 8.16. We emphasize that if the counterpoise correction is not applied, the BSSE leads to a large discrepancy, especially for smaller basis sets. Interestingly, even though the energy gap closes with the larger basis sets, it remains as wide as +10 kJ mol^{-1} at the QZVPP level, because higher angular momentum functions are required to close that gap. Even at the QZVPP level the basis set limit is not reached. The best obtained result, corresponding to def2-QZVPP+2f basis set, is -33.41 kJ mol^{-1}. This value is expected to be close to the basis set limit for the MP2 method.

$P[AuPH_3]_4^+$ cation: To find the source of discrepancy in the preferred structure, we first investigated the difference in ΔE=$E(C_{4v})$-$E(T_d)$ due to the two different 19-VE pseudopotentials of Andrae, used by Pyykkö *et al.*, and the one of Figgen, applied by Fang and Wang. We found the difference to be negligible. Only at the QZVPP level does it exceed 1 kJ mol^{-1}. The choice of the PP also does not affect the symmetry of the cation. The more general aspects of PP influence on the Au(I)-Au(I) interaction have already been investigated by Pyykkö *et al.*[75,76,86]

We then turned our attention to the basis sets. We found that, in the case of the older Karlsruhe basis sets (def-X), especially the smaller sets are too poor in higher angular momentum basis-functions to properly describe the closed-shell aurophilic interactions. Augmentation with two contracted f-functions (-B) yields mainly negative ΔE values, with C_{4v} symmetry preferred. By adding the two uncontracted f-functions (-A), the

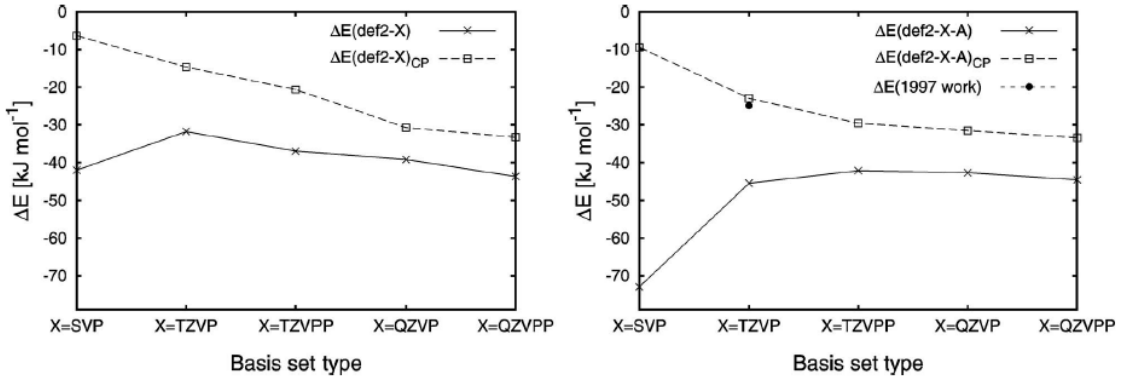

Figure 8.16: Comparison of the calculated, noncounterpoise-corrected ΔE and corrected ΔE_{CP} values for $[ClAuPH_3]_2$ dimer, obtained using original def2-X Karlsruhe and augmented def2-X-A bases (-A stands for two *un*contracted f-functions, α=0.20, 1.19).

convergence level is achieved already at the TZVP level (see Fig. 8.17).

The latest generation of basis sets (def2-X) contains at least one f-function (α=0.72) on gold, even for the smallest def2-SVP basis set. Although the application of newer basis sets lowers the calculated ΔE, as compared to the corresponding older def-X sets, the f-subspace is still too small, and additional enrichment with more f-functions is helpful. As expected, it also is better to add two uncontracted f-functions rather than keep them contracted.

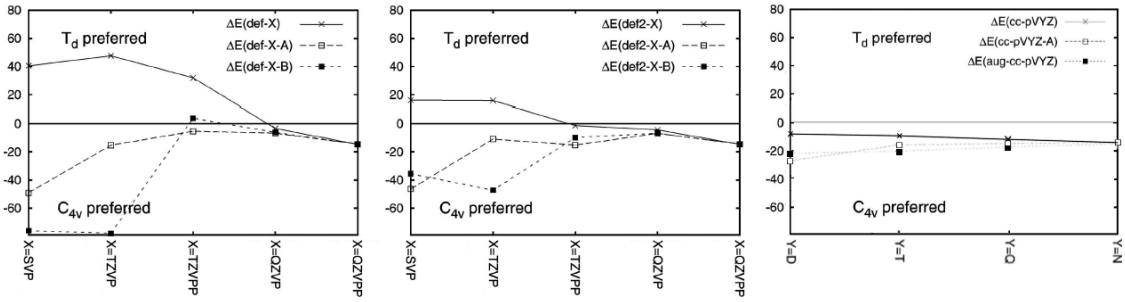

Figure 8.17: The comparison of calculated ΔE=$E(C_{4v})$-$E(T_d)$ energies for $[P(AuPH_3)_4]^+$ ion, obtained using the original split-valence (def-X and def2-X) and correlation-consistent (cc-pVYZ) basis sets, with the ΔE values obtained in the same sets augmented with two uncontracted (-A) and two contracted (-B) f-type functions ($\alpha = 0.20, 1.19$).

In the case of both def-X and def2-X basis sets, adding the two f-functions to the smallest SVP sets, will lead to a large overestimation of ΔE, even by a factor of 4 (see Fig. 8.17, left and center). The larger sets contain already enough higher angular momentum functions (f and higher). The addition of two extra f-functions does not make a substantial difference. It also explains why the ΔE values obtained previously by Pyykkö and co-workers were more negative. Most likely, the employed basis sets were still too small to give results close to the convergence limit. Nevertheless, the qualitative results of the previous studies are reconfirmed.

Our currently best estimate for ΔE, calculated with largest Karlsruhe split-valence

basis sets, is -15.0 kJ mol^{-1}. It is in good agreement with the calculations performed with the correlation-consistent basis sets (Fig. 8.17, right). For the cc basis sets, we also performed the two-point basis-set extrapolation[87] based on the total energies calculated for the T_d and C_{4v} isomers. The ΔE calculated at the basis-set limit is estimated to -14.5 kJ mol^{-1}. Finally, the comparison with the value of -13.74 kJ mol^{-1} calculated with the full cc-pV5Z basis, yields a satisfactory agreement. Both the results obtained with the split-valence and the cc type basis sets, converge to the similar result.

In none of the studied cases were we able to reproduce the positive value of ΔE=+84 kJ mol^{-1} reported by Fang and Wang.[83] The C_{4v} symmetry is still favored at the MP2 level.

SCS-MP2: $[ClAuPH_3]_2$ dimer

It is known that MP2 method tends to overestimate aurophilic attraction. For certain small cases, such as the 'classical' dimer model (see Fig. 8.15), it is still possible to calculate the interaction energy, $\Delta E_{CP}(R)$, even at the Coupled-Cluster level.

Fig. 8.18 illustrates a comparison of high-accuracy Coupled-Cluster results with those calculated using standard MP2 and the recently introduced SCS-MP2 method. We emphasize an excellent agreement between the CCSD(T) and much less expensive SCS-MP2 results.

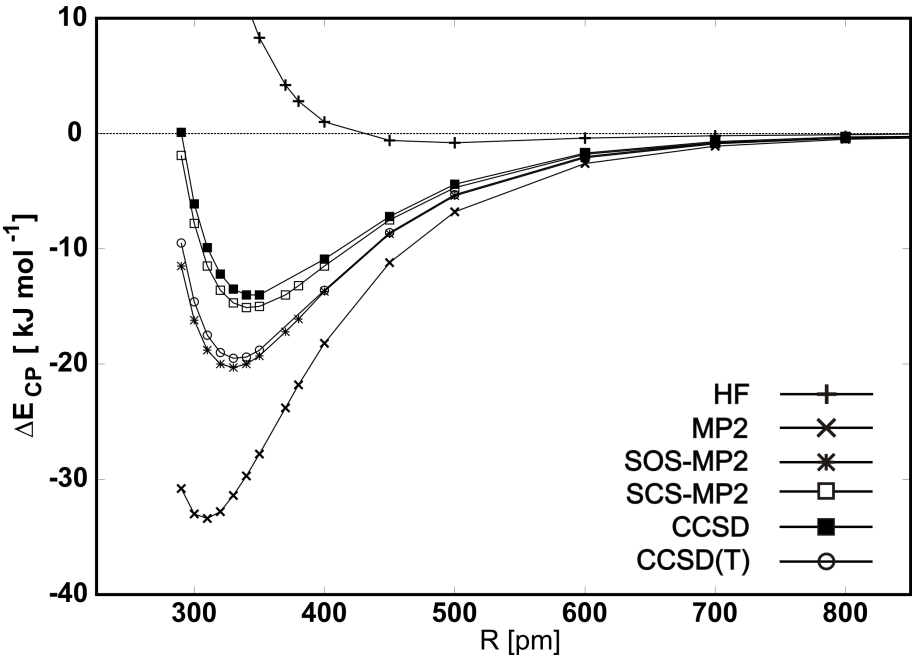

Figure 8.18: A comparison of CC methods with standard MP2 and empirically corrected SOS-MP2 and SCS-MP2 methods.

SCS-MP2: $[P(AuPH_3)_4]^+$ cation

Following the observation that the Spin-Component-Scaled MP2 results for the $[ClAuPH_3]_2$ dimer are in a significantly better agreement with CCSD(T) than with the MP2 ones, we have recalculated the ΔE=$E(C_{4v})$-$E(T_d)$ using the SCS-MP2 scheme.

Using a sufficiently large, split-valence quadruple-zeta quality basis sets, we reproduced our earlier result for MP2 (ΔE=-16.2 kJ mol^{-1}). The SCS-MP2 yields ΔE=+19.8 kJ mol^{-1} and the SOS-MP2 yields ΔE=+37.8 kJ mol^{-1}. Both methods favor T_d symmetry.

8.4 High-accuracy calculations of MCN, M=Cu-Au

The AuCN molecule is important because it is related to the $[Au(CN)_2]^-$ ion, which is used in most of the gold production in the world. It is also interesting from the point of view of this thesis, as AuCN and similar cyanides can be considered as monomers in the formation of 2D crystals discussed in Paper I. Experimental studies on *solid* MCN (M=Cu, Ag, Au) exist.[88,89,90,91] Molecular calculations were reported by Boldyrev *et al.*,[92] Dietz *et al.*,[93] Grotjahn *et al.*,[94] Lee *et al.*,[95] Veldkamp *et al.*[96] and Schwerdtfeger *et al.*[97]

Experimental structural data for *gas-phase* AuCN have been reported recently.[98] Understanding the qualitative aspects of molecular bonding was thus of interest. Our calculated M-C bond lengths are only slightly larger than the sum of the triple-bond covalent radii[99] indicating complex, multiple-bond character of that bond. For most accurate results, we applied Coupled-Cluster theory. We compare those with results from commonly used second-order Møller-Plesset perturbation approach (MP2). Similar calculations, have appeared but with relatively small basis sets. We now performed both MP2 and CCSD(T) calculations using the newest pseudopotentials[82] for the metal and large basis sets.[100]

An example on AuCN

Level of electron correlation: Table 8.5 summarizes results obtained by the MP2 and CCSD(T) methods. We found that the MP2 method fails to describe the AuCN molecule accurately. The Au-C distance obtained using a cc-pVQZ basis set deviates from the experimental value by -2.5 %, while the CCSD(T) one is in much better agreement with experiment. For the C-N distance, MP2 also is worse than CCSD(T). Similar relative trends were found for the CuCN and AgCN molecules [Paper V].

Effect of freezing the core: The gold cyanide molecule with 19-VE Au and all-electron C and N has 16 occupied molecular orbitals. In order to save computational time, one would typically freeze some, or all, of the six occupied MOs below the ten top ones in Fig. 8.19. From below, they are MO_1 $1s_C$, MO_2 $1s_N$, MO_3 $5s_{Au}$, and the

Method	Basis/frozen MOs	Au-C	C-N	ω_1	ω_2	ω_3
CCSD(T)	cc-pVQZ/none	191.12	116.23	2215	289	482
	cc-pVQZ/MO_{1-2}	191.26	116.50	2203	284	480
	cc-pVQZ/MO_{1-3}	191.14	116.50	2203	285	481
	cc-pVQZ/MO_{1-6}	192.10	116.50	2202	278	471
Expt. (g)	Ref.[98]	191.22519(84)	115.86545(97)	-	320	480

Table 8.4: Selected calculated bond lengths [pm] and harmonic vibrational modes [cm^{-1}] for MCN (M=Cu, Ag, Au)

Method/Case		Au-C	C-N	ω_1	ω_2	ω_3
AuCN						
CCSD(T)	cc-pVDZ	191.85	118.31	2183	282	486
	cc-pVTZ	190.97	116.50	2214	292	481
	cc-pVQZ	191.12	116.23	2215	289	482
MP2	cc-pVDZ	187.63	118.95	2096	298	521
	cc-pVTZ	186.41	117.16	2128	312	520
	cc-pVQZ	186.51	116.92	2127	309	520
Expt. (g)	Ref.[98]	191.22519(84)	115.86545(97)	-	320	480
Expt. (s)	Ref.[88]	197.175	115.474	-	-	-
AgCN						
CCSD(T)	cc-pVDZ	201.52	118.40	2172	240	406
	cc-pVTZ	202.16	116.59	2201	234	397
	cc-pVQZ	202.04	116.33	2203	221	402
Expt. (g)	Ref.[98]	203.1197(23)	116.0260(26)	-	240	400
Expt. (s)	Ref.[89]	206.00	116.00	-	-	-
CuCN						
CCSD(T)	cc-pVDZ	180.49	118.49	2172	305	492
	cc-pVTZ	181.96	116.66	2203	262	479
	cc-pVQZ	181.85	116.39	2204	255	483
Expt. (g)	Ref.[98]	182.962(4)	116.213(3)	-	270	478
Expt. (s)	Ref.[90]	184.60	117.00	2170	-	-

Table 8.5: Selected calculated bond lengths [pm] and harmonic vibrational modes [cm^{-1}] for MCN (M=Cu, Ag, Au)

three MO_{4-6} $5p_{Au}$. The effect of freezing selected electrons in AuCN is summarized in Table 8.4. Unfreezing the $5p_{Au}$ shortens the Au-C distance by 1 pm. Deeper excitations have a small effect. The C-N distance is not affected by 'opening' the Au orbitals. It is shortened by as much as 0.3 pm if the MO_{1-2} are correlated as well. The effect on the Au-C-N bend, ω_2, parallels that on the Au-C distance. The stretching ω_3 is influenced by opening the $5p_{Au}$. The C-N stretch, ω_1, is increased by 13 cm^{-1} if the 1s shells, MO_{1-2}, are correlated.

Basis-set-size effect: The errors of the calculated Au-C and C-N distances clearly diminish from DZ to TZ basis. The errors diminish even further from TZ to QZ and the smallness suggests adequate convergence (Table 8.5). Change from the smallest, cc-pVDZ, to the largest cc-pVQZ basis lowers the relative errors roughly by a factor of 7 for both Au-C and C-N distances. The CCSD(T) harmonic vibrational frequencies, calculated with the three basis sets of different quality, yield a similar picture. For the C-N stretch, not even an experimental estimate is available. Because the rotational spectroscopy gives the vibrational wavenumbers only indirectly, the experimental values

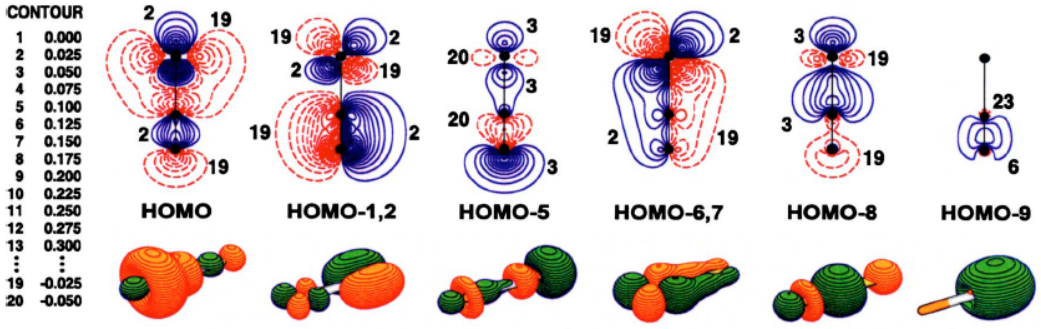

Figure 8.19: The ten highest occupied Hartree-Fock MO, of AuCN. The Kohn-Sham MOs look very similar. The bottom row depicts orbitals important for bonding.

of ω_2 and ω_3 are only rough estimates.

Spin-orbit effects: The calculations with spin-orbit effects, obtained at the DFT level, yield bond lengths in good agreement with the known experimental values and also with the present CCSD(T) calculations. The spin-orbit effects on bond lengths are small and rise to -0.38 pm for the Au-C distance in AuCN. The magnitude grows with the nuclear charge of the metal atom.

Anharmonicity: The experimental estimates reported by Okabayashi *et al.* for MCN (M=Cu, Ag, Au) are based on the harmonic approximation, hence the good agreement with calculated CCSD(T) harmonic values. We estimated the error introduced by the harmonic approximation at the MP2 level using cc-pVTZ basis sets (Paper V, Table VII). In each case, the anharmonicities lower the calculated frequency. The anharmonic correction, Δ, decreases strongly with Z. In case of the C-N stretch, Δ is approximately -33 cm^{-1} and remains constant for all analyzed cyanides.

Qualitative bonding analysis: The experimental M-C (M=Cu, Ag, Au) are only a few picometers longer than those predicted by the triple-bond covalent radii (by 3, 6, and 8 pm). Among the occupied MOs depicted in Fig. 8.19 we indeed find the bonding orbitals HOMO-6,7. The higher-lying HOMO-1 and HOMO-2 is basically the cyanide π. Interestingly, the Au-C bonding occurs both in the HOMO, and there primarily to the gold 'doughnut' hybrid, and in the lower-lying HOMO-8.

Our *best-estimated* results for studied cyanides are presented in Table 8.6. The M-C distances agree with experiments within about 0.6 pm or even better. The M-C bond-length trend for the four metals is Cu < Rg < Au < Ag. We emphasize the significance of the BSSE. The remaining difference may come from the r_s, r_e, and the r_m definitions, the pseudopotential approximation, coupled-clusters perturbative triplets, or other sources. Our calculated harmonic frequencies are expected to be more accurate than available gas-phase experimental estimates.[94,98]

Metal	Cu	Ag	Au
M-C	181.85	202.04	191.12
BSSE	+0.52	+0.47	+0.31
SO	-0.01	-0.09	-0.38
Best est.	182.36	202.42	191.05
Expt.	182.962(4)[c]	203.1197(23)[d]	191.22519(84)[d]
C-N	116.39	116.33	116.23
SO	+0.01	+0.07	0.00
Best est.	116.40	116.40	116.23
Expt.	116.213(3)[c]	116.0260(26)[d]	115.86545(97)[d]
ω_1			
Best CCSD(T)[a]	2204	2203	2215
Best est.	2171	2171	2181
Expt. est.	-	-	-
Expt. est. + Δ	-	-	-
ω_3			
Best CCSD(T)[a]	255	221	289
Best est.	232	209	285
Expt. est.	270[c]	240[d]	320[d]
Expt. est. + Δ	247	228	316
ω_3			
Best CCSD(T)[a]	483	402	482
Best est.	439	378	472
Expt. est.	478[c]	400[d]	480[d]
Expt. est. + Δ	434	376	470

[a]CCSD(T)/cc-pVQZ, [b]PBE-ZORA/QZ4P, [c]Ref.,[94] [d]Ref.[98]

Table 8.6: The best estimated values for bond lengths and vibrational harmonc modes for MCN (M=Cu, Ag, Au).

References

[1] Pyykkö, P. *Angew. Chem. Int. Ed.* **2004,** *43,* 4412.

[2] Häkkinen, H. *Chem. Soc. Rev.* **2008,** *37,* 1847.

[3] Møller, C.; Plesset, M. S. *Phys. Rev.* **1934,** *46,* 618.

[4] Pople, J. A.; Binkley, J. S.; Seeger, R. *Int. J. Quant. Chem.* **1976,** *10,* 1.

[5] Schwabe, T.; Grimme, S. *Acc. Chem. Research* **2008,** *41,* 569.

[6] Grimme, S. *J. Chem. Phys.* **2003,** *118,* 9095.

[7] Langhoff, S. R.; Davison, E. R. *Int. J. Qunat. Chem.* **1974,** *8,* 61.

[8] Pople, J. A.; Head-Gordon, M.; Raghavachari, K. J. *J. Chem. Phys.* **1987,** *87,* 5968.

[9] Mazziotti, D. A. *Phys. Rev. Letters* **2004,** *93,* 213001.

[10] Hohenberg, P.; Kohn, W. *Phys. Rev.* **1964,** *136,* B864.

[11] Kohn, W.; Sham, L. J. *Phys. Rev.* **1965,** *140,* A1133.

[12] Becke, A. D. *Phys. Rev. A* **1986,** *33,* 2786.

[13] Perdew, J. P.; Burke, K.; Ernzerhof, M. *Phys. Rev. Letters* **1996,** *77,* 3865.

[14] Becke, A. D. *Phys. Rev. A* **1988,** *38,* 3098.

[15] Lee, C.; Yang, W.; Parr, R. G. *Phys. Rev. B* **1988,** *37,* 785.

[16] Vosko, S. H.; Wilk, L.; Nusair, M. *Can. J. Phys.* **1980,** *58,* 1200.

[17] Tao, J.; Perdew, J. P.; Staroverov, V. N.; Scuseria, G. E. *Phys. Rev. Letters* **2003,** *91,* 146401.

[18] Perdew, J. P.; Kurth, S.; Zupan, A.; Blaha, P. *Phys. Rev. Letters* **1999,** *82,* 2544.

[19] Alloutia, F.; Mancerona, L.; Alikhani, M. E. *J. Mol. Struc.* **2009,** *903,* 4.

[20] Görling, A.; Levy, M. *Phys. Rev. B* **1993,** *47,* 13105.

[21] Görling, A.; Levy, M. *Phys. Rev. A* **1994,** *50,* 196.

[22] Schwabe, T.; Grimme, S. *Phys. Chem. Chem. Phys.* **2007,** *9,* 3397.

[23] Koch, W.; Holthausen, M. C. *A Chemist's Guide to Density Functional Theory;* Wiley-VCH: Weinheim,.

[24] Ibach, H. *Solid-State Physics, An Introduction to Principles of Materials Science;* Springer-Verlag: 1996.

[25] Chadi, D. L.; Cohen, M. L. *Phys. Rev. B* **1973,** *8,* 5747.

[26] Monkhorst, H. J.; Pack, J. D. *Phys. Rev. B* **1976,** *13,* 5188.

[27] Born, M.; Oppenheimer, R. *Ann. Phys. (Leipzig)* **1927,** *84,* 457.

[28] Stanke, M.; Kedziera, D.; Bubin, S.; Adamowicz, L. *J. Chem. Phys.* **2007,** *127,* 134107.

[29] Stanke, M.; Komasa, J.; Kedziera, D.; Bubin, S.; Adamowicz, L. *Phys. Rev. A* **2008,** *77,* 062509.

[30] Valeev, E. F.; Sherrill, C. D. *J. Chem. Phys.* **2003,** *118,* 3921.

[31] Francis, G. P.; Payne, M. C. *J. Phys. Cond. Matt.* **1990,** *2,* 4395.

[32] Martin, J. M. L.; Taylor, P. R. *Chemical Physics Letters* **1994,** *225,* 473 - 479.

[33] Martin, J. M. L.; Taylor, P. R. *Chemical Physics Letters* **1996,** *248,* 336 - 344.

[34] Martin, J. M. L. *Chemical Physics Letters* **1995,** *242,* 343 - 350.

[35] Levine, I. N. *Quantum Chemistry;* Prentice-Hall: 1991.

[36] Helgaker, T.; Klopper, W.; Tew, D. P. *Mol. Phys.* **2008,** *106,* 2107.

[37] Dunlap, B. I.; Connolly, J. W. D.; Sabin, J. R. *J. Chem. Phys.* **1979,** *71,* 3396.

[38] Bethe, H. A.; Salpeter, E. E. *Quantum Mechanics of One- and Two-Electron Atoms;* Plenum Press: 1977.

[39] Douglas, M.; Kroll, N. M. *Ann. Phys.* **1974,** *82,* 89.

[40] Jansen, G.; Hess, B. A. *Phys. Rev. A* **1989,** *39,* 6016.

[41] Barysz, M. *J. Chem. Phys.* **2001,** *114,* 9315.

[42] Reiher, M.; Wolf, A. *Relativistic Quantum Chemistry, The Fundamental Theory of Molecular Science;* Wiley-VCH: Weinheim, 2009.

[43] Dyall, K. *J. Chem. Phys.* **1997,** *106,* 9618.

[44] Filatov, M.; Cramer, D. *J. Chem. Phys.* **2003,** *118,* 7641.

[45] Barysz, M.; Sadlej, A. J. *J. Chem. Phys.* **2003,** *116,* 2696.

[46] Kutzelnigg, W.; Liu, W. *J. Chem. Phys.* **2005,** *123,* 241102.

[47] Zhdanov, G. S.; Shugam, E. A. *Zh. Fiz. Khim.* **1945,** *19,* 519.

[48] Hakala, M. O.; Pyykkö, P. *Chem. Comm.* **2006,** *2006,* 2890.

[49] Wang, H. M. J.; Lin, I. J. B. *Organometallics* **1998,** *17,* 972.

[50] Vaughan, L. G. *J. Am. Chem. Soc.* **1970,** *92,* 730.

[51] Vaughan, L. G. *J. Organomet. Chem.* **1980,** *190,* C56.

[52] Naumkin, F. *Phys. Chem. Chem. Phys.* **2006,** *8,* 2539.

[53] Gibson, J. K. *J. Vac. Sci. Technol.* **1998,** *16,* 653.

[54] Pyykkö, P.; Patzschke, M.; Suurpere, J. *Chem. Phys. Letters* **2003,** *381,* 45.

[55] Sneed, M. C.; Maynard, J. L.; Brasted, R. C. *Comprehensive Inorganic Chemistry, Vol. 2;* D. van Nostrand Co., Inc.: , 1954.

[56] Rykova, E. A.; Zaitsevskii, A.; Mosyagin, N. S.; Isaev, T. A.; Titov, A. V. *J. Chem. Phys.* **2006,** *125,* 241102.

[57] Wesendrup, R.; Laerdahl, J. K.; Schwerdtfeger, P. J. *Chem. Phys.* **1999,** *110,* 9457.

[58] Gillespie, R. J.; Granger, P.; Morgan, K. R.; Schrobilgen, G. J. *Inorg. Chem.* **1984,** *23,* 887.

[59] Kertesz, M.; Guloy, A. M. *Inorg. Chem.* **1987,** *26,* 2852.

[60] Cutforth, B. D.; Gillespie, R. J.; Ireland, P.; Sawyer, J. F.; Ummat, P. K. *Inorg. Chem.* **1983,** *22,* 1344.

[61] Brown, I. D.; Gillespie, R. J.; Morgan, K. R.; Sawyer, J. F.; Schmidt, K. J.; Tun, Z.; Ummat, P. K. *Inorg. Chem.* **1987,** *26,* 689.

[62] Catalano, V. J.; Malwitz, M. A.; Noll, B. C. *Chem. Commun.* **2001,** *2001,* 581.

[63] Furche, F.; Ahlrichs, R.; Weis, P.; Jacob, C.; Gilb, S.; Bierweiler, T.; Kappes, M. M. J. *Chem. Phys.* **2002,** *117,* 6982.

[64] Den Hartog, J. P. *Mechanical Vibrations;* McGraw-Hill: New York, London, 1947.

[65] Hoppe, R. *J. Reine Angew. Math.* **1871,** *73,* 158.

[66] Love, A. E. H. *Proc. London Math. Soc.* **1893,** *24,* 118.

[67] Ceulemans, A.; Vos, I. *Mol. Phys.* **1991,** *72,* 1051.

[68] Ceulemans, A.; Fowler, P. W.; Vos, I. *J. Chem. Phys.* **1994,** *100,* 5491.

[69] Schmidbaur, H.; Graf, W.; Müller, G. *Angew. Chem.* **1988,** *100,* 439.

[70] Melnik, M.; Parish, R. V. *Coord. Chem. Rev.* **1986,** *70,* 157.

[71] Scherbaum, F.; Grohmann, A.; Huber, B.; Krüger, C.; Schmidbaur, H. *Angew. Chem.* **1988,** *100,* 1602.

[72] Schmidbaur, H. *Gold Bull.* **1990,** *23,* 11.

[73] Jiang, Y.; Alvarez, S.; Hoffmann, R. *Inorg. Chem.* **1985,** *24,* 749.

[74] Pyykkö, P.; Zhao, Y.-F. *Angew. Chem.* **1991,** *103,* 622 Angew. Chem. Int. Ed. Engl., **30**, 604, (1991).

[75] Pyykkö, P.; Runeberg, N.; Mendizabal, F. *Chem. Eur. J.* **1997,** *3,* 1451.

[76] Pyykkö, P.; Mendizabal, F. *Chem. Eur. J.* **1997,** *3,* 1458.

[77] Runeberg, N.; Schütz, M.; Werner, H.-J. *J. Chem. Phys.* **1999,** *110,* 7210.

[78] Li, J.; Pyykkö, P. *Chem. Phys. Letters* **1992,** *197,* 586.

[79] Magnko, L.; Schweizer, M.; Rauhut, G.; Schütz, M.; Stoll, H.; Werner, H.-J. *Phys. Chem. Chem. Phys.* **2002,** *4,* 1006.

[80] Li, J.; Pyykkö, P. *Inorg. Chem.* **1993,** *32,* 2630.

[81] Andrae, D.; Häußermann, U.; Dolg, M.; Stoll, H.; Preuß, H. *Theor. Chim. Acta* **1990,** *77,* 129.

[82] Figgen, D.; Rauhut, G.; Dolg, M.; Stoll, H. *Chem. Phys.* **2005,** *311,* 227.

[83] Fang, H.; Wang, S.-G. *J. Phys. Chem. A.* **2006,** *111,* 1562.

[84] Zeller, E.; Beruda, H.; Kolb, H.; Bissinger, A.; Riede, P.; Schmidbaur, J. *Nature* **1991,** *352,* 141.

[85] Pyykkö, P.; Tamm, T. *Organometallics* **1998,** *17,* 4842.

[86] Pyykkö, P.; Mendizabal, F. *Inorg. Chem.* **1998,** *37,* 3018.

[87] Helgaker, T.; Jørgensen, P.; Olsen, J. *Molecular Electronic-Structure Theory;* Wiley: Chichester, 2000.

[88] Hibble, S. J.; Hannon, A. C.; ; Cheyne, S. M. *Inorg. Chem.* **2003,** *42,* 4724.

[89] Hibble, S. J.; Cheyne, S. M.; Hannon, A. C.; Eversfield, S. G. *Inorg. Chem.* **2002,** *41,* 1042.

[90] Hibble, S. J.; Cheyne, S. M.; Hannon, A. C.; Eversfield, S. G. *Inorg. Chem.* **2002,** *41,* 4990.

[91] Bowmaker, G. A.; Kennedy, B. J.; Reid, J. C. *Inorg. Chem.* **1998,** *37,* 3968.

[92] Boldyrev, A. I.; Li, X.; Wang, L.-S. *J. Chem. Phys.* **2000,** *112,* 3627.

[93] Dietz, O.; Rayón, V. M.; Frenking, G. *Inorg. Chem.* **2003,** *42,* 4977.

[94] Grotjahn, D. B.; Brewster, M. A.; Ziurys, L. M. *J. Am. Chem. Soc.* **2001,** *124,* 5895.

[95] Lee, D.; Lim, I. S.; Lee, Y. S.; Hagebaum-Reignier, D.; Jeung, G.-H. *J. Chem. Phys.* **2007,** *126,* 244313.

[96] Veldkamp, A.; Frenking, G. *Organometallics* **1993,** *12,* 4613.

[97] Schwerdtfeger, P.; Boyd, P. D. W.; Burrell, A. K.; Taylor, M. J. *Inorg. Chem.* **1990,** *29,* 3593.

[98] Okabayashi, E. Y.; Okabayashi, T.; Koto, F.; Tanimoto, M. *Presented at the 61st Ohio State University International Symposium on Molecular Spectroscopy, Columbus, OH, 2006, Paper No. RE09.* .

[99] Pyykkö, P.; Riedel, S.; Patzschke, M. *Chemistry* **2005,** *11,* 3511.

[100] Peterson, K. A.; Puzzarini, C. *Theor. Chem. Acc.* **2005,** *114,* 283.